



Design of Effective Grouting Pattern in Kerman Water Conveyance Tunnel Using DFN-DEM and Analytical Approaches

Sasan Ghorbani¹ · Komeil Bour² · Roohollah Javdan³ · Mohammad Bour⁴

Received: 13 December 2022 / Accepted: 25 March 2023 / Published online: 3 April 2023
© The Author(s), under exclusive licence to Springer Nature Switzerland AG 2023

Abstract

The main purpose of this study is to determine the appropriate grouting pattern for sealing the fractures of the Kerman Water Conveyance Tunnel (KWCT) using the discrete fracture network-discrete element method (DFN-DEM) and analytical approaches. In the first stage, nine DFNs were generated with different fracture densities. Following that, the hydraulic conductivity values were calculated to determine the representative elementary volume (REV) of a geological section of the KWCT. The grout's effective radius in the optimal size blocks was then determined. Analytical models based on joint features and different rheological properties of the grout were also used to evaluate the grout penetration length. Finally, the most suitable patterns of grouting boreholes in rock masses with low and high fracture densities at a pressure of 24 bar were obtained by borehole arrangement with angles of 60° and 45°, respectively. These patterns were effectively used as the optimal injection arrangement in a zone of the KWCT that was at high risk of water inrush. Following the grouting, some core samples were drilled to assess the grouting efficiency and check the condition of the solidified grout in the rock mass cracks. According to the observations, the proposed arrangements were extremely efficient.

Keywords Grout injection · DFN-DEM approach · Rheological properties · REV

Introduction

High water inflow may lead to difficult construction and working conditions in tunneling. Grouting has been widely used to reduce water inflow into rock masses for decades [1]. Among these, grout injection has played a vital role in a wide range of underground projects for different purposes. For instance, grouting can be essential in tunnel construction to enhance the stability of a tunnel by improving the stiffness of the surrounding rock mass and reducing the hydraulic conductivity and water inflow that may threaten the stability [2, 3]. Furthermore, poor TBM performance is a result of

groundwater inflow problems caused by excavation in the mixed ground [4–6].

Grouting performance is influenced not only by the rock mass properties and geological conditions but also by the grout material and grouting process [1]. In the meantime, selecting the appropriate injection pressure, the optimal spacing of the injection holes, and generally, the appropriate pattern of injection holes are all parts of the design of a proper injection operation. The performance of grout injection can be intensely dependent on the joint conditions surrounding the rock mass [7]. When the individual joint is poor due to low intensity, short length, and low permeability, injection results are unsuitable because the designed injection zone is not filled with injected grout. In contrast, when a joint set is predominantly developed in a certain direction, the injected grout may not penetrate optimally through the connected joints in the designed injection zone. Therefore, injection performance is uneconomical [2, 8].

Various studies have been carried out to investigate grout propagation and determine the effective radius of the grout. Butrón et al. [9] have presented a new pre-excavation grouting method using water pressure tests (WPTs) and pressure–volume time (PVT) recordings for

✉ Sasan Ghorbani
sasan.ghorbani@mi.iut.ac.ir

¹ Department of Mining Engineering, Isfahan University of Technology, 84156-83111, Esfahan, Iran

² Department of Mining Engineering, Faculty of Engineering, Tarbiat Modares University, Tehran, Iran

³ Faculty of Mining, Petroleum and Geophysics Engineering, Shahrood University of Technology, Shahrood, Iran

⁴ Faculty of Civil Engineering, University of Guilan, Guilan, Iran

the permeation grouting to reduce the water inflow into a railway tunnel. Their proposed method successfully reduced the transmissivity and improved rock characterization. Saeidi et al. [10] carried out a numerical simulation to predict grout flow and penetration length into the jointed rock mass using UDEC software. Mortazavi and Maadikhah [11] investigated the effects of important factors on the grout flow in rock masses by numerical method. Their results show that grout penetration depth increases with increasing joint aperture, normal stiffness, and grouting pressure. In contrast, the grout penetration depth decreases with increasing in situ stress and pore water pressure. Mohajerani et al. [12] developed a computationally efficient algorithm to model the fluid grout propagation in 2D DFNs. Zou et al. [13] investigated the cement grout propagation in water-saturated 2D DFNs by extending a two-phase flow model for Bingham fluids in a single saturated fracture. It was found that the network structure and hydraulic variability significantly affect the grout propagation in 2D DFN systems.

In general, based on the literature review, it has been determined that there is still no documented method that can calculate step-by-step the optimal arrangement of injection holes in the grout injection operation in the tunnel. Hence, this paper attempted to determine the grout's effective radius and the suitable arrangement of injection boreholes in the Kerman Water Conveyance Tunnel (KWCT) project using the DFN-DEM and analytical approaches. The reason for using these approaches is the highly jointed environment of the KWCT. Additionally, all previous studies show that the grout propagation in rock joints and the prediction of grout's penetration length have been the topic of many investigations. With regard to the grouting design, it is beneficial to have an accurate assessment of the grout's penetration length in order to design a suitable arrangement of the grout injection boreholes. Additionally, in this work, the analytical solution was used to calculate the grout's penetration length in joints. Finally, field observations and measurements in a hydrogeological zone of the southern lot of KWCT were used to better understand the results of the proposed arrangement of injection boreholes and real-world conditions of the grouting process. In this research, the appropriate arrangement of injection boreholes has been systematically analyzed using three approaches, such as numerical, analytical, and field observations, and it has been tried to be more complete than in previous studies.

Research Methodology

In this study, five steps were followed to determine the suitable arrangement of injection boreholes in the KWCT.

- First, the hydraulic conductivity and the representative elementary volume (REV) size of the rock mass in the KWCT project were investigated using the DFN-DEM approach.
- After determining the REV size of the numerical models, the cement grout propagation and the effective radius in fracture networks were analyzed.
- In addition to numerical simulations, the grout penetration length has also been investigated by analytical solutions.
- The injection boreholes pattern on the KWCT segment was designed using the grout's effective radius.
- Finally, the proposed arrangement's efficiency was evaluated in one of the tunnel's southern lots, which was faced with a water inrush.

The workflow in this study is also shown in detail in Fig. 1.

Numerical Solution of Cement Grout Propagation in the Jointed Rock Mass

Determining the grout's effective radius is one of the most significant challenges in designing the grout injection process. So far, some experimental studies have been performed to simulate grout penetration length in single fractures [14–16]. However, due to the complex networks of the rock mass including fractures with random distributions, it is impossible to determine the grout's effective radius using experimental methods. In this regard, the discrete fracture network (DFN) model has been applied to simulate groundwater flow and solute transport in fractured rocks both in 2D and 3D [13].

Numerical methods can be a good tool for modeling the actual fluid flow in the rock mass with complex fracture networks. Accordingly, various researchers have always considered numerical methods in injection studies in the rock mass. In recent years, various numerical methods have been used to model grout injection. In the meantime, the DEM method can analyze the fluid flow and cement grouting simulation through the fractures of a system of impermeable blocks. Therefore, the required parameters for tunnel injection operations, such as grout's effective radius, borehole spacing, and finally, the appropriate pattern of grout injection boreholes, can be determined by generating discrete fracture networks (DFN) of rock mass and using discrete element software (DFN-DEM approach).

Determination of REV in 2D DFN Models

Due to the fact that the large-scale in situ tests are difficult and time-consuming and there are also limitations in experiment equipment, the numerical methodology should

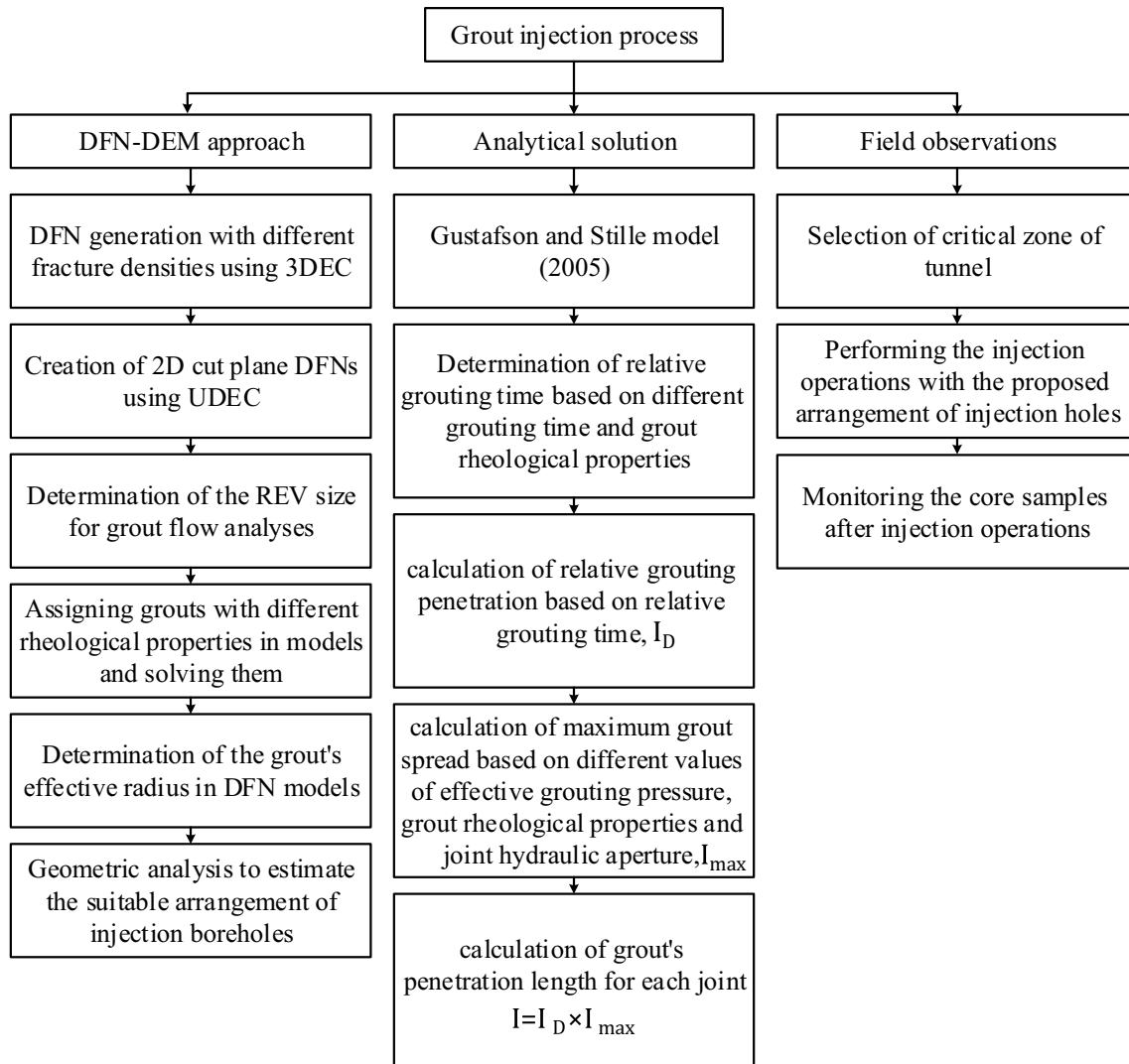


Fig. 1 Flowchart of applied methodology

be taken into account as a remedy. One useful technique to represent the overall equivalent properties of fractured rocks in field scales is to use the concept of the representative elementary volume (REV) [17]. Hence, determining the REV of the jointed rock mass based on its hydraulic conductivity is the first step in simulating grout flow and estimating its effective radius. To calculate the flow rate, the hydraulic conductivity, and then the REV size of jointed rock mass, it is necessary to first create a discrete fracture network that can express the geometric properties of the fracture.

The stochastic DFN approach is one of the crucial techniques widely used in rock engineering studies. The general stochastic DFN approach assumes fractures to be straight lines (in 2D) or planar disks/polygons (in 3D) and treats the other geometrical properties (such as position, frequency,

size, orientation, and aperture) as independent random variables [18].

The stochastic DFN models were generated by 3DEC software to represent the fractured rock masses in the first stage of this research, and the generated geometry was then used to create a DEM model for numerical analyses using the UDEC code. In other words, 2D-DFN models were extracted from 3D-DFNs to determine the hydraulic conductivity of rock mass.

Fractures that do not affect the calculation of the properties and behavior of the rock mass and are known as “non-persistent” fractures are deleted in UDEC software after the generation of joints in DFN models. In other words, the DFN models were regularized before the analyses by removing isolated and dead-end fractures.

After regularization of the DFN models, the hydraulic aperture values are assigned for each individual fracture, and the mass continuity equations are then established at the fracture intersections for fluid flow between intersections. Since the purpose of the calculations in this study is to evaluate the directional permeability of the DFN models, steady-state flow with a generic hydraulic boundary condition with the constant hydraulic gradient in the x and y -directions is assumed (Fig. 2) [19].

Darcy’s Law can be used to determine the equivalent permeability (hydraulic conductivity) tensor of the cut plane after preparing the DFN models [Eq. (1)].

$$Q = K.A.\Delta H \tag{1}$$

where Q is the flow rate vector, K is the permeability tensor (hydraulic conductivity), ΔH is the head gradient vector, and A is the width that the fluid flows through. Also, $q = Q/A$ is the flow rate through a unit cross-sectional area. Thus, Darcy’s Law can be rewritten as Eq. (2).

$$q = K.\Delta H \tag{2}$$

Finally, from matrix theory, the permeability tensor can be then obtained from Eq. (3). The details of calculation for fluid flowing in 2D DFNs are described in the previous work of Zhang et al. [20].

$$\begin{bmatrix} K_{xx} & K_{xy} \\ K_{yx} & K_{yy} \end{bmatrix} = \begin{bmatrix} q_{xx} & q_{xy} \\ q_{yx} & q_{yy} \end{bmatrix} \begin{bmatrix} 1/\Delta P_x & 0 \\ 0 & 1/\Delta P_y \end{bmatrix} \tag{3}$$

Theoretical Background on Grout Flow in Joints in 2D DFN Models

In the current study, UDEC is employed to simulate grout flow through joints. UDEC is a 2D numerical program based on the distinct element method. In general, the UDEC code is suitable when the flow is mainly governed through a network of joints.

The flow of a Bingham body (or liquid), such as cement grout, is of the viscoplastic type. The major difference between this model and that of a Newtonian liquid is that, for a Bingham fluid, yield stress (τ_0), must be exceeded to initiate flow. To simulate the viscous grout fluid, the Bingham flow model was employed in this study. In UDEC, fluid flow governing equations for steady laminar flow of a Bingham fluid was calculated based on Buckingham’s equation [21] for a rectangular channel as Eq. (4).

$$Q = \frac{1}{\mu} \left[-\frac{\Delta P}{12L} a^3 + \frac{\tau_0^3}{3\left(\frac{\Delta P}{L}\right)^2} - \frac{\tau_0 a^2}{4} \right] \tag{4}$$

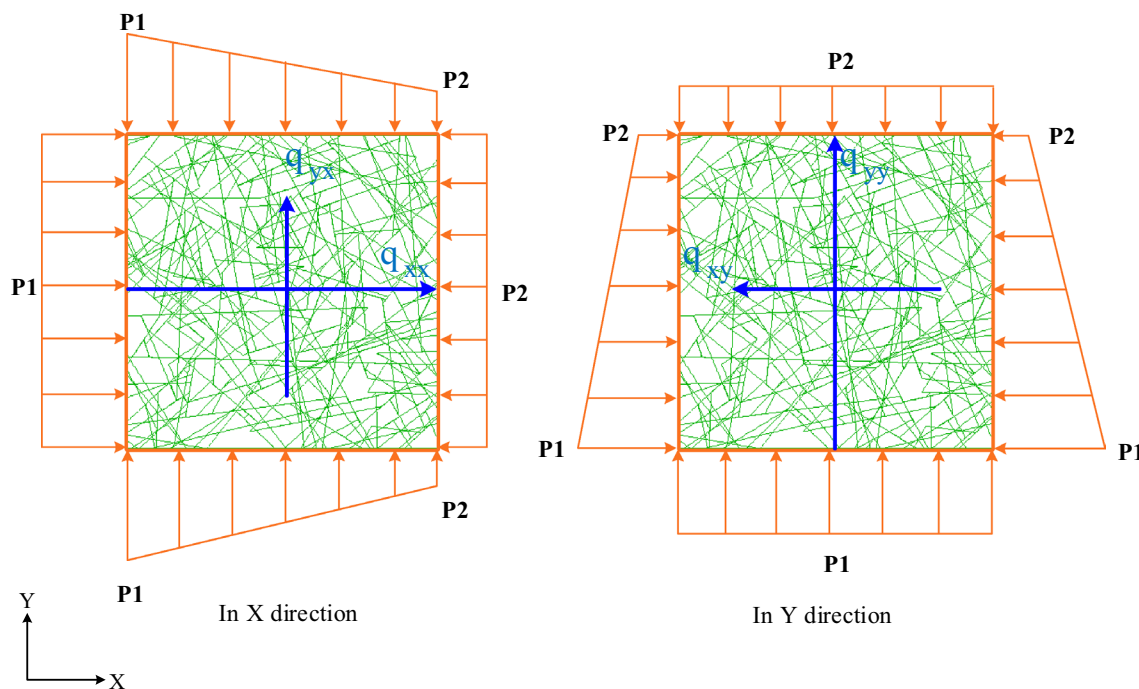


Fig. 2 Boundary conditions for the determination of the hydraulic conductivity of the fractured rock mass

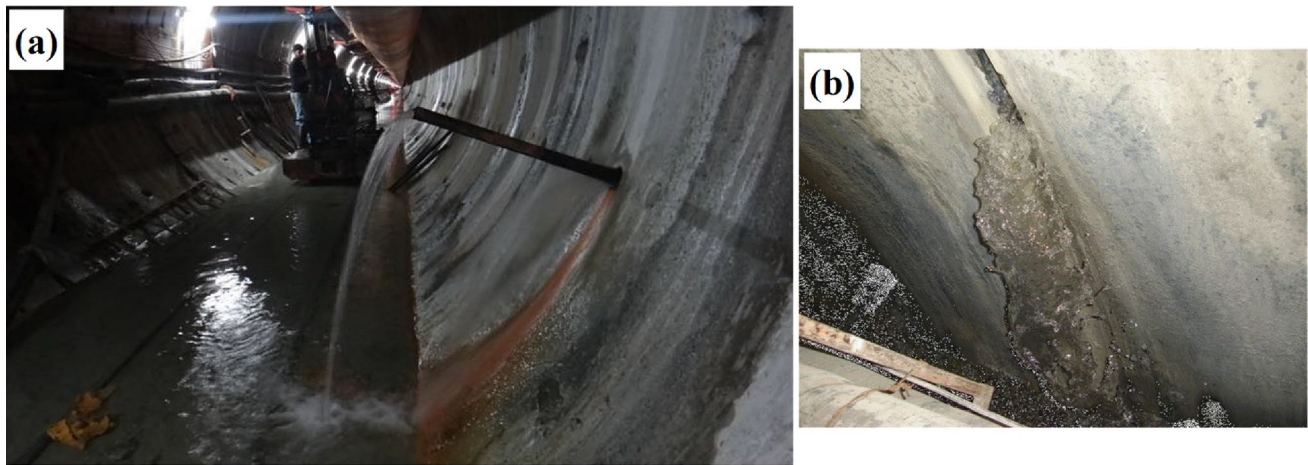


Fig. 3 Water inflow into the section of KWCT

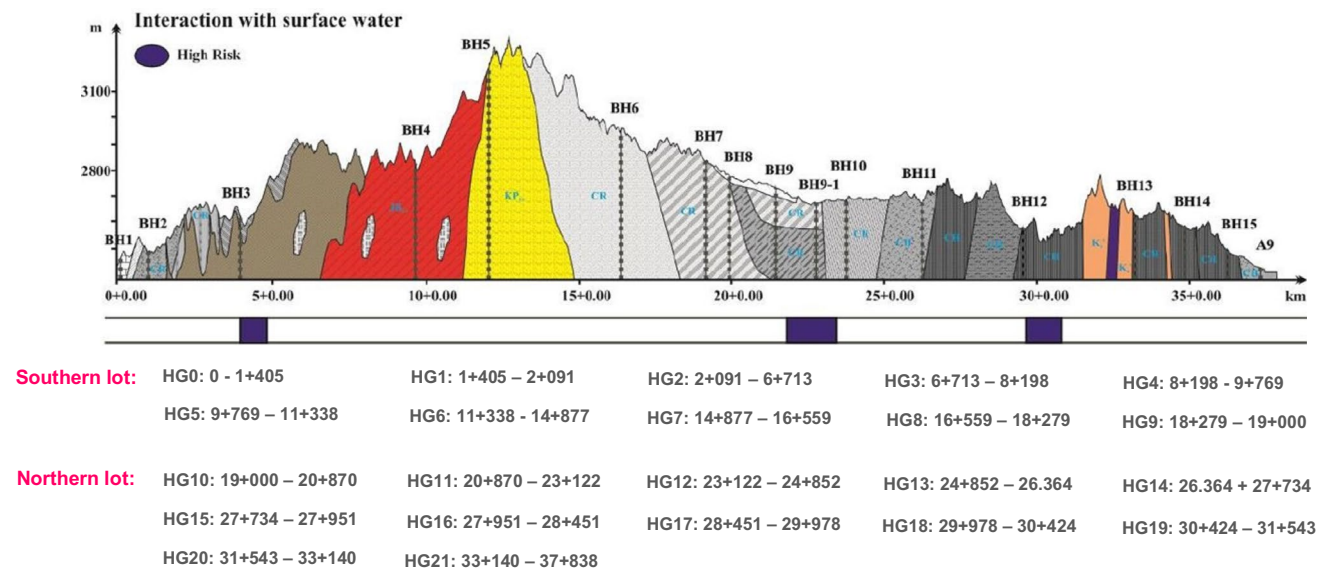


Fig. 4 Profile of the interaction with surface water in the KWCT project

where Q is the flow rate per unit width of the joint, μ is the viscosity of Bingham fluid, and $\Delta P/L$ is the pressure gradient.

Analytical Solutions of Cement Grout Propagation in the Jointed Rock Mass

In addition to the DFN-DEM approach, analytical solutions can be used to investigate the grout’s effective radius and consequently the reduction of water inflow into the tunnel. The expected water inflow to a tunnel is dependent on geometry, location, water pressure, rock mass geological, hydrogeological conditions, thickness, and hydraulic conditions of the grouted zone. The inflow could be calculated using Eq. (5) for deep tunnels without a grouted

zone (deep-located tunnel: the tunnel is located more than approximately 3–4 times the tunnel diameter). In addition, in tunnels with a grouted zone, the inflow is affected by the grouted zone’s conductivity K_g as well as the thickness of the grouted zone (I). The inflow could then be calculated with Eq. (6). Finally, Eq. (7) has been used to calculate the required sealing effect (SE) [22].

$$q_{\text{ungrouted}} = \frac{2 \times \pi \times K}{\ln\left(\frac{2 \times H}{R_t}\right) + \xi} \tag{5}$$

$$q_{\text{grouted}} = \frac{2 \times \pi \times K_g \times H}{\ln\left(\frac{R_t + I}{R_t}\right) + \frac{K_g}{K} \times \ln\left(\frac{2 \times H}{R_t + I}\right) + \frac{K_g}{K} \times \xi} \tag{6}$$



Fig. 5 Core samples of the drilled boreholes in the zone HG11

Sealing Effect (%)

$$= 100 \times \frac{\text{Inflow without grouting} - \text{Inflow with grouting}}{\text{Inflow without grouting}} \quad (7)$$

where q : Flow per meter of the tunnel [m^3/s] K : Initial hydraulic conductivity [m/s], H : Water pressure [m], R_t : Radius of the tunnel [m], ξ : Skin factor (For engineering purposes, a value of 2–5 for tunnels is recommended [23]) I : Thickness of the grouted zone [m], K_g : Hydraulic conductivity of the grouted zone [m/s].

Also, the penetration length of the cement grout in a joint can be calculated with the analytical solution of Gustafson and Stille [24]. The earliest version of the analytical solution to determine the penetration length [Eq. (8)], does not provide realistic results. Because the calculated penetration length was based on an infinite time. While in the injection operation in the tunnel, the grouting time in the boreholes is limited. Therefore, Gustafson and Stille [24] modified their analytical solution to provide a more realistic estimate for

grout penetration length by incorporating the concept of characteristic grouting time (t_0) as a key parameter for grout injection. They defined the relative penetration length (I_D) and the relative time (t_D) using Eqs. (9)–(11). Therefore, after determining the I_D and t_D , the penetration length of each joint is calculated using Eq. (12). Finally, it can be concluded that the penetration length is a function of different rock mass and grout properties where it may be expressed as Eq. (13).

$$I_{\max} = \frac{\Delta P_g}{2\tau_0} \times \frac{e_m^2}{\text{JRC}^{2.5}} \quad (8)$$

$$I_D = \frac{I}{I_{\max}} \quad (9)$$

$$\left\{ \begin{array}{l} t_D = \frac{t}{t_0} \\ t_0 = \frac{6\Delta P\mu_g}{\tau_0^2} \end{array} \right\} \rightarrow t_D = \frac{t \times \tau_0^2}{6\Delta P\mu_g} \quad (10)$$

$$I_D = \sqrt{\left(\frac{t_D}{2(0.6 + t_D)}\right)^2 + 4\left(\frac{t_D}{2(0.6 + t_D)}\right) - \frac{t_D}{2(0.6 + t_D)}} \quad (11)$$

Equations (7)–(10)

$$\begin{aligned} \rightarrow I &= I_D \times I_{\max} \\ &= \left[\sqrt{\left(\frac{t_D}{2(0.6 + t_D)}\right)^2 + 4\left(\frac{t_D}{2(0.6 + t_D)}\right) - \frac{t_D}{2(0.6 + t_D)}} \right] \\ &\quad \times \left(\frac{\Delta P_g}{2\tau_0} \times \frac{e_m^2}{\text{JRC}^{2.5}} \right) \end{aligned} \quad (12)$$

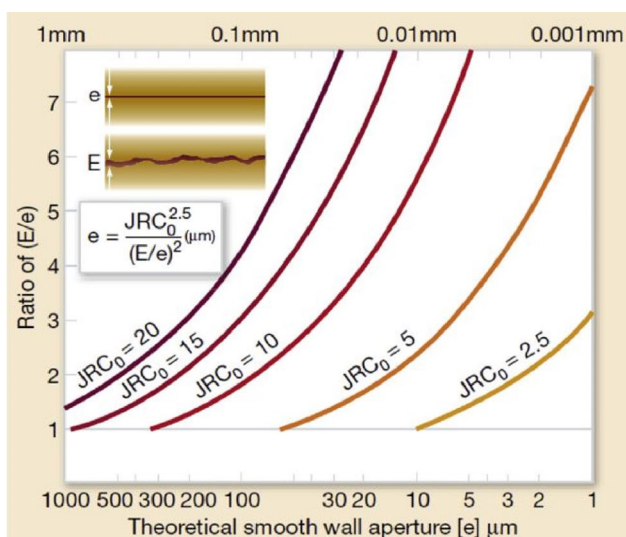


Fig. 6 The relevance between e , E , and JRC values [34]

$$I = f[e_h(e_m, JRC), \Delta P, t, \mu_g, \tau_0] \tag{13}$$

where I is the actual penetration length, I_{max} is the maximum penetration length, ΔP_g is the effective grouting pressure ($\Delta P_g = P_g - P_w$), e_h is the effective hydraulic aperture of the joint, e_m is the mechanical or physical joint aperture, τ_0 is the yield shear strength, t is the actual grouting time, and μ_g is the grout viscosity.

Case Study Features

The Kerman water conveyance tunnel project in the south-east of Iran, Kerman province, at a base level of ~2370 m and length of ~38 km, is one of the longest tunnels in the volcanic area in the world. This tunnel has a total length of 37.9 km and comprises a northern 18.9 km length and a southern 19.0 km portion [25].

The KWCT project aims to provide part of the required water for Kerman city from Safa Dam to Kerman city. This tunnel is divided into two lots, southern and northern, with the finished diameters and boring diameters of 4.5 m, 5.275 m, and 3.9 m, 4.665 m, respectively. The boring of these two lots has been done with two double-shield TBMs. The tunnel is circular, with a maximum overburden point of 940 m in the tunnel’s central area.

Table 1 Rock and fracture parameters

Property	Value
Intact rock	
Density	$\rho_R = 2200 \text{ kg/m}^3$
Elastic modulus	$E_R = 3 \text{ GPa}$
Poisson’s ratio	$\nu_R = 0.32$
Tensile strength	$\sigma_{tR} = 3 \text{ MPa}$
Cohesion	$C_R = 16 \text{ MPa}$
Friction angle	$\phi_R = 41^\circ$
Fracture	
Normal stiffness	$JK_n = 10 \text{ GPa/m}$
Shear stiffness	$JK_s = 10 \text{ GPa/m}$
Friction angle	$\phi_f = 30^\circ$
Initial aperture	$a_0 = 2 \text{ mm}$
Residual aperture	$a_{res} = 0.1 \text{ mm}$

The Problem in the KWCT Project

Groundwater is one of the essential factors in the design and stabilization of tunnels. Nowadays, estimating the groundwater flow rate into tunnels is of particular importance. Water can flow into the tunnel on the tunnel face and between the segments [see Fig. 3(a) and (b)]. The water inflow of the tunnels will cause numerous problems for the personnel, machinery, wall stability, and tunnel roof. Undoubtedly, the

Fig. 7 Calculated values of hydraulic apertures based on values of e_m and JRC

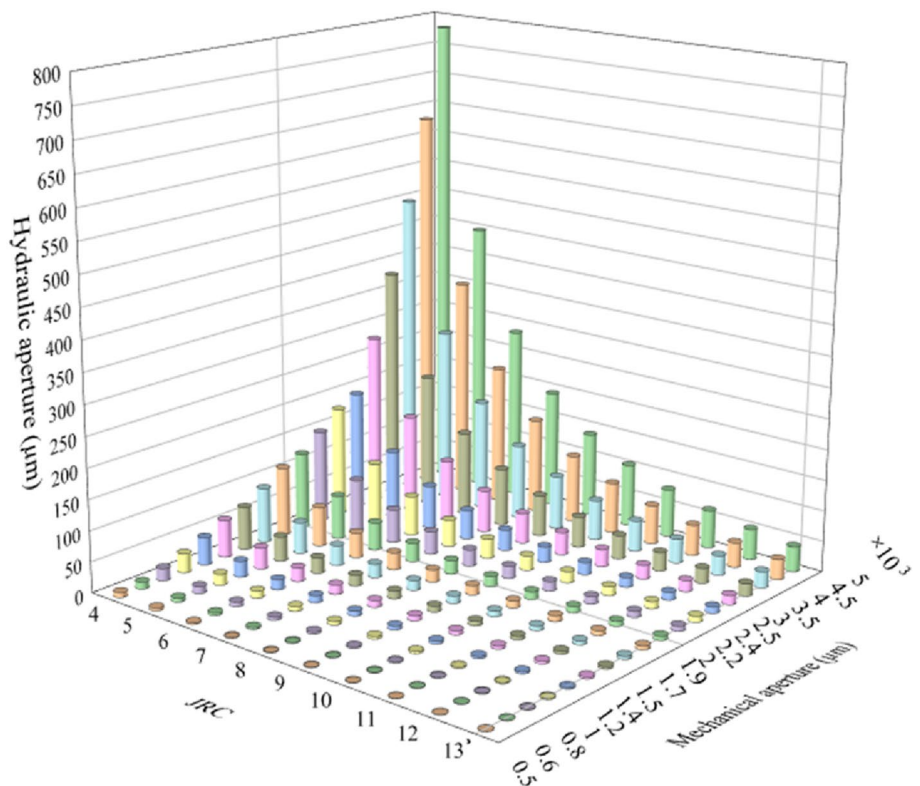


Table 2 Three mixing designs of grout for the analyses of grout penetration length

Properties	Design		
	A	B	C
W/C ratio	1:1	0.8:1	0.5:1
Cement weight (Kg)	750	800	1212
Water (Lit)	750	640	606
Bentonite (Kg)	35	35	35
Density (Kg/m ³)	1535	1675	1853
Viscosity (Pa s)	0.007	0.015	0.027
Yield shear strength (Pa)	3	8.3	23.2

Table 3 Used empirical equations to determine the injection pressure in the KWCT (equations adopted from [19])

Criteria	Equation	Value (bar)
Leepald	$P = 36.765 \times 10^{-3} \times H$	2.6
American criteria	$P = 0.025 \times H$	1.75
European criteria	$P = 0.1 \times H$	7
Weaver	$P = 22.62 \times 10^{-3} \times H$	1.6

Table 4 Fracture parameters used for 3D-DFNs generation

Joint set	Dip D (°)	Dip direction DD (°)	Fisher's constant K (%)	Fracture intensity P ₂₀ (m ⁻²)
1	71	185	4.24	0.4, 0.8, 1.2
2	36	304	9.61	0.4, 0.8, 1.2
3	60	84	10.83	0.4, 0.8, 1.2

inflow of water into tunnels under construction is one of the issues that may have destructive effects on drilling operations (for example, reducing drilling rates) and ultimately affect tunneling activity. Therefore, it is necessary to predict the location and amount of water inflow into the tunnel and make arrangements to deal with it. So, groundwater control in both tunnel construction and operation stages is one of the most critical tunnel design and control challenges. As shown in Fig. 4, there is a high risk of surface water interaction along the KWCT route in three sections. However, the risk of colliding with surface water is the greatest from 22 to 23.5 km (zone HG11). Therefore, in this study, the selection of a suitable injection pattern in this section has been investigated. The hydrogeological status has also been investigated in order to determine the high-risk zones along the tunnel route. The information from drilled boreholes in the study area was used to investigate the groundwater status and hydrogeological conditions. Therefore, the tunnel route's northern section was divided into 12 hydrogeological

zones. Finally, high-risk zones were introduced along the tunnel route where water inflow is more likely.

Geomechanical Properties of Rock Mass

The design of an injection operation, including selecting the appropriate grout, injection pressure, spacing, direction of injection boreholes, and in general, the optimal pattern of injection boreholes depends on the geo-mechanical characteristics of the injection environment. According to the geological and geotechnical investigation (borehole, core logging, and laboratory testing), the rock masses in the KWCT route have been classified as consisting of 21 lithography types in both lot 1 and lot 2. Core samples from drilled boreholes have been used to determine the intact rock properties. Figure 5 shows core samples from drilled boreholes in zone HG11 at various depths. Furthermore, the values of the intact rock and fracture properties are listed in Table 1.

Mechanical and Hydraulic Apertures of Joints

One of the most important parameters in grout injection operations in tunnels is the hydraulic aperture. The mean hydraulic apertures (e_h or e) will need conversion to mean mechanical apertures (e_m or E) using estimates of the small-scale roughness JRC. The relevance between mechanical and hydraulic apertures and JRC values is presented in Eq. (14) [26, 27]. The curves illustrated in Fig. 6, show the predicted relation between (e_m/e_h) and hydraulic aperture (e_h) for different values of JRC.

$$e_h = \frac{e_m^2}{JRC^{2.5}} \quad (14)$$

In this study, the mechanical apertures and JRC of the joints in zone HG11 of KWCT are in the range of 0.5–5 mm and 4–13, respectively. Therefore, to determine the grout penetration length in the joints using analytical methods, the values of hydraulic apertures must be determined according to Eq. (14). As shown in Fig. 7, hydraulic apertures have been calculated for each joint using specified e_m and JRC values. As a result of the calculations, joints with a mechanical aperture of 5 mm and a JRC of 4 have the highest hydraulic aperture values.

Grout Material Properties

The most common grout mixture to seal the rock and soil is cement-based material. In rock grouting, the most important factors of penetration grouting include a water-to-cement ratio (W/C), yield value, the grain size of cement paste, viscosity, and setting time [10, 28]. Grout rheology behavior

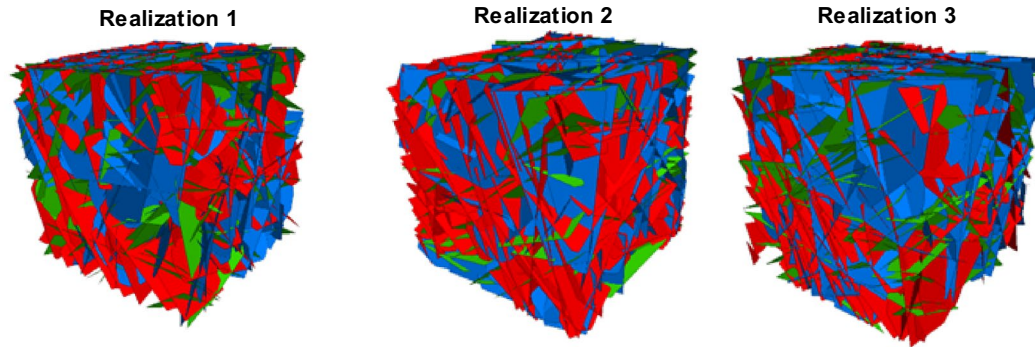
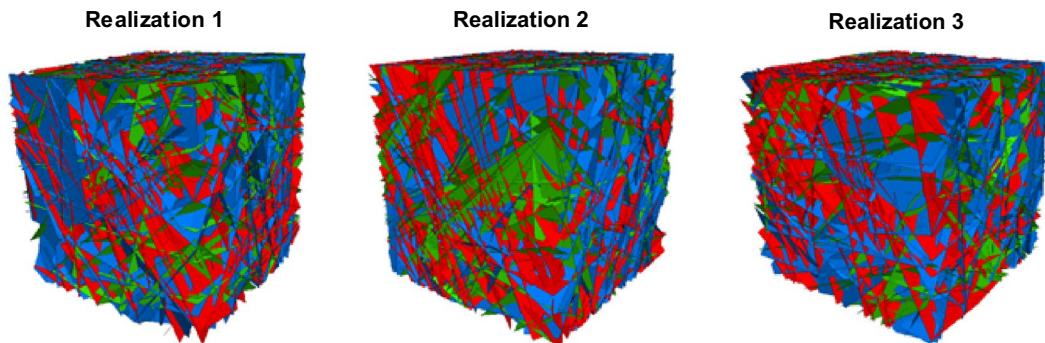
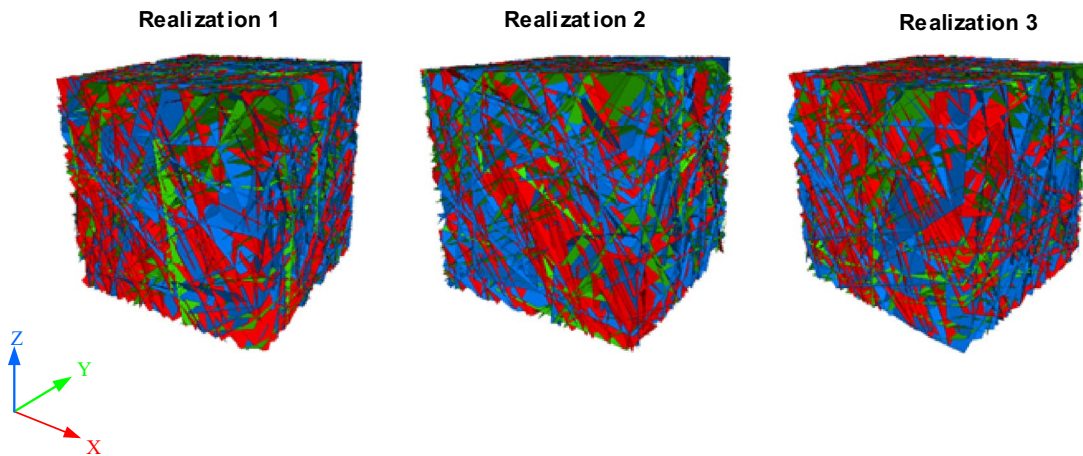
(a) $P_{20} = 0.4 \text{ m}^{-2}$ (b) $P_{20} = 0.8 \text{ m}^{-2}$ (c) $P_{20} = 1.2 \text{ m}^{-2}$ 

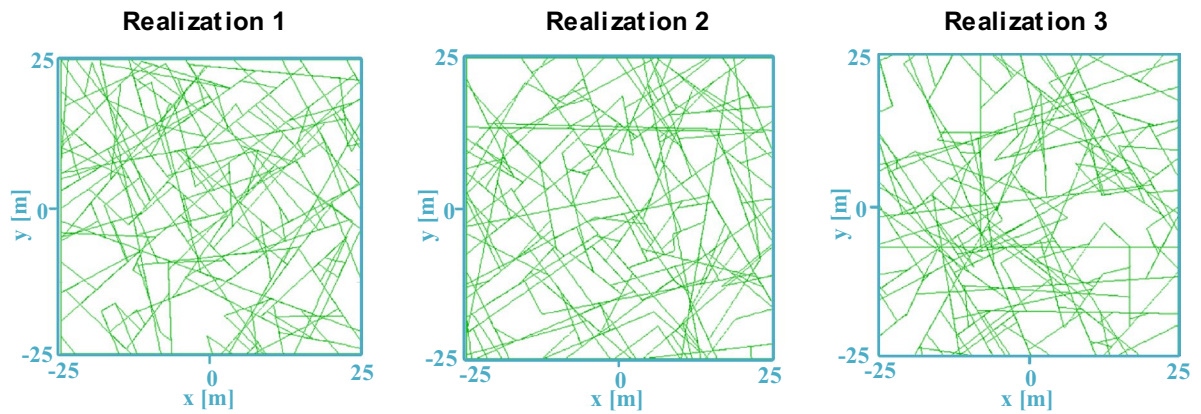
Fig. 8 Different realizations of the discrete fracture network for **a** $P_{20} = 0.4 \text{ m}^{-2}$, **b** $P_{20} = 0.8 \text{ m}^{-2}$ and **c** $P_{20} = 1.2 \text{ m}^{-2}$

plays a vital role in the injection process because it determines the relationship between pressure and flow rate.

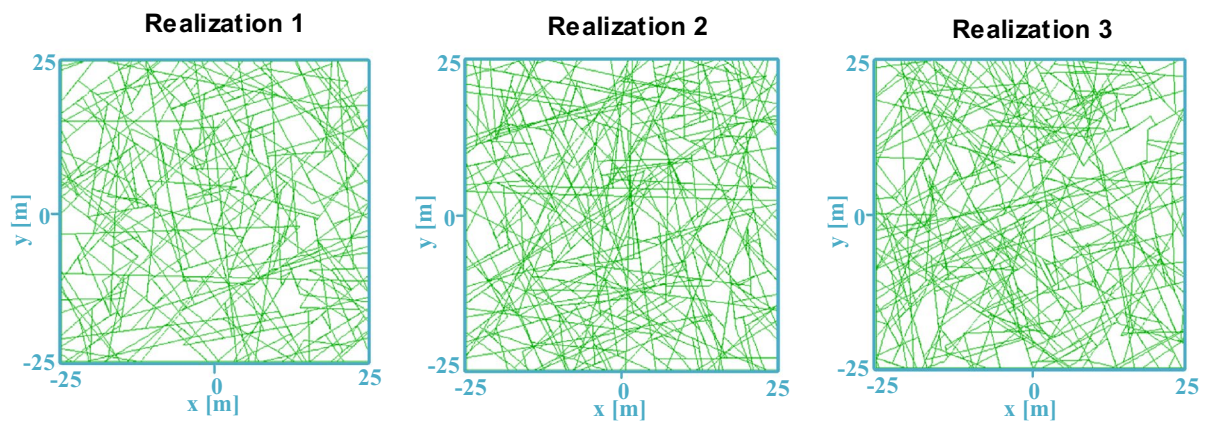
Grout flow has been widely simulated using a Bingham fluid model which is characterized by yield shear strength and dynamic viscosity. In this kind of fluid, the yield shear

strength has to be overcome to initiate flow such that the grout behaves as a rigid body at low stress but starts to flow as a viscous fluid at high stress [2, 29]. The rheological feature of the grout is a function of the type of cement and the water-to-cement ratio. A specific behavioral model must be

(a) $P_{20} = 0.4 \text{ m}^{-2}$



(b) $P_{20} = 0.8 \text{ m}^{-2}$



(c) $P_{20} = 1.2 \text{ m}^{-2}$

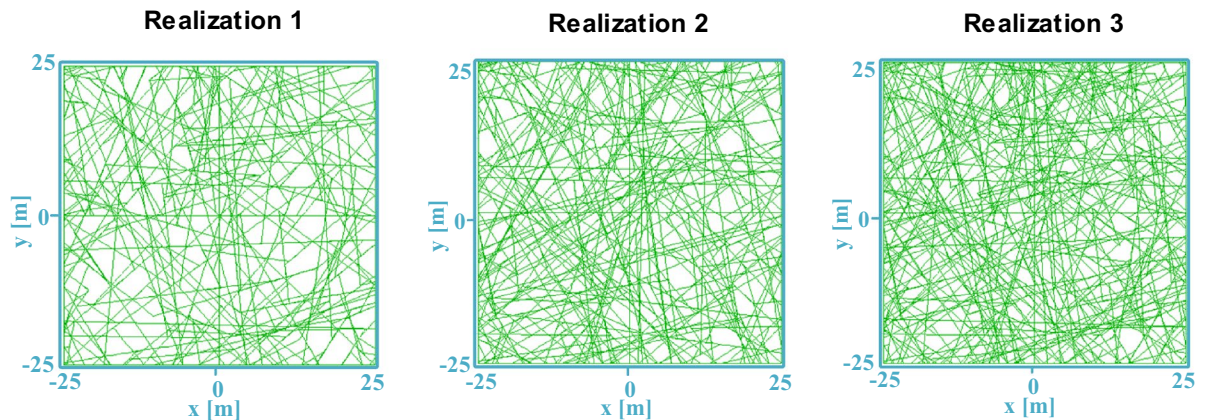


Fig. 9 Extracted DFNs from the 3D model and transformed in the UDEC with different fracture densities

considered for the scope of application of each type of grout material. Three mixing designs are considered for numerical and analytical analyses in this study (Table 2). As shown

in this table, three different mixing designs, have different properties, such as water-to-cement ratio, viscosity, and yield shear strength.

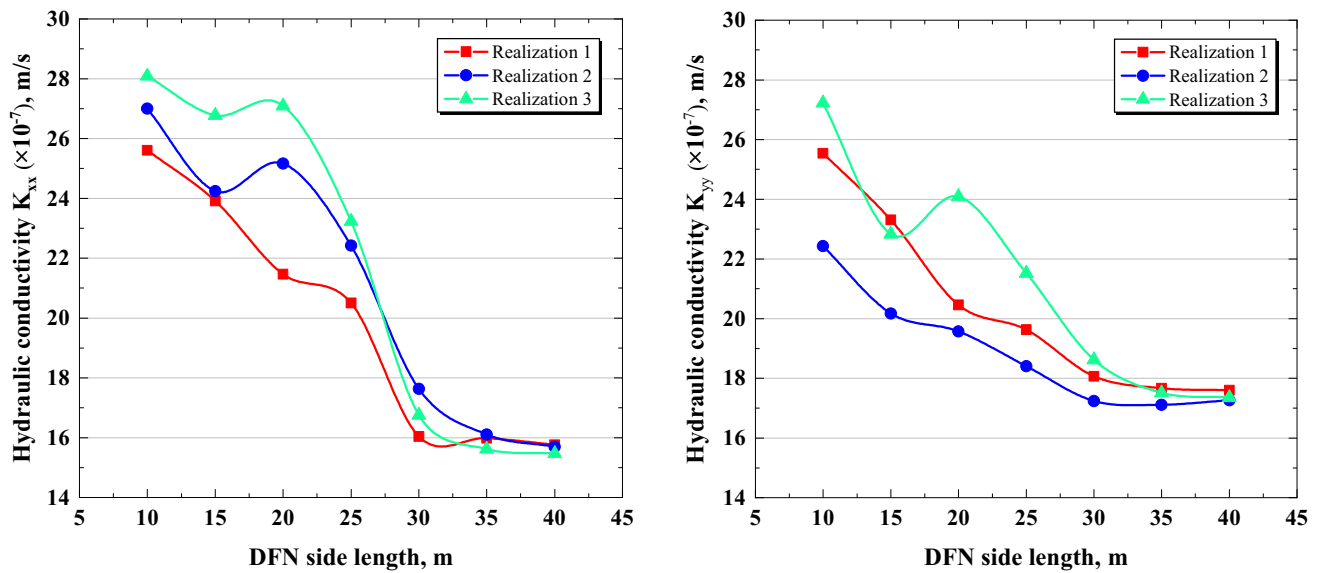


Fig. 10 Hydraulic conductivity (K_{xx} and K_{yy}) with F.D=0.4

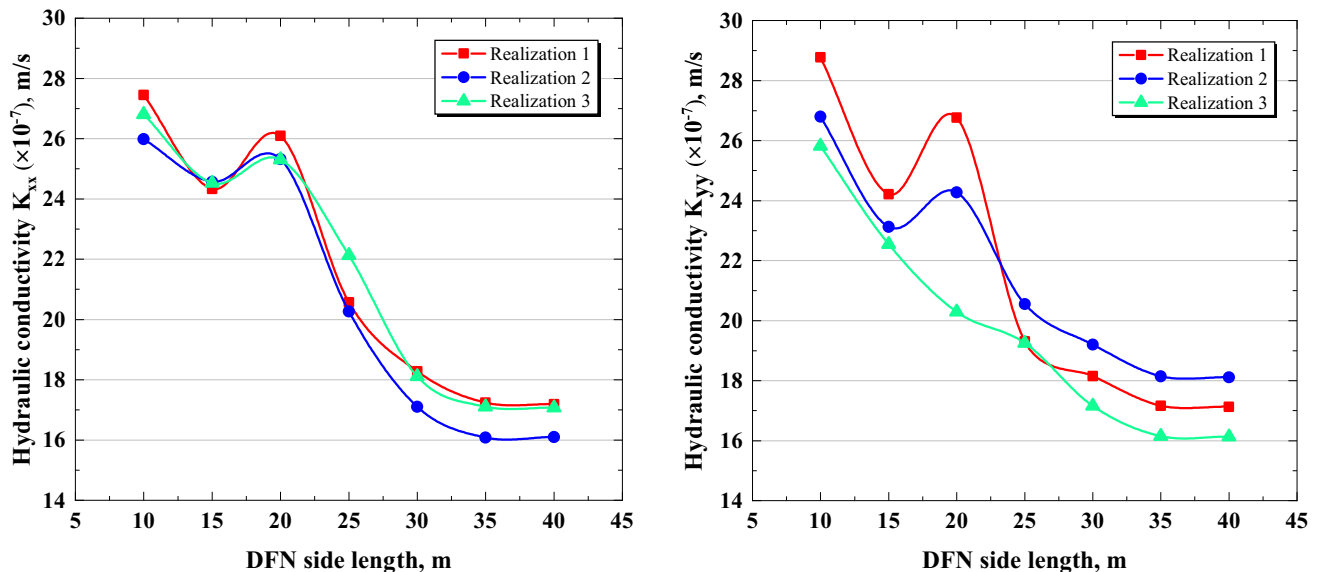


Fig. 11 Hydraulic conductivity (K_{xx} and K_{yy}) with F.D=0.8

Grout Injection Pressure

The grouting pressure is the most critical technical parameter that affects the grouting process [11]. The maximum acceptable amount of grouting pressure is introduced as the allowable pressure, which must always be less than the allowable pressure during the injection operation. Because of the complicated equations that govern the environment, determining this parameter for each section is practically impossible. Hence, it is usually obtained from empirical relationships [19]. So, the equations and graphs provided by various researchers, which are determined based on the

depth of the injection boreholes, were used to select the appropriate injection pressure. After using the mentioned equations to determine the injection pressure, an average estimate of the values obtained in the studied zone was proposed and used in numerical and analytical solutions.

The depth required for injection varies based on the amount of water leakage. The borehole depth in areas where water leakage is not high is 4 m. In areas where leakage water inflow into the tunnel is high (collision with fault and crushed areas or groundwater aquifers), according to the diameter tunnel of 4.66 m in the northern part, the length of injection holes can be considered up to 7 m

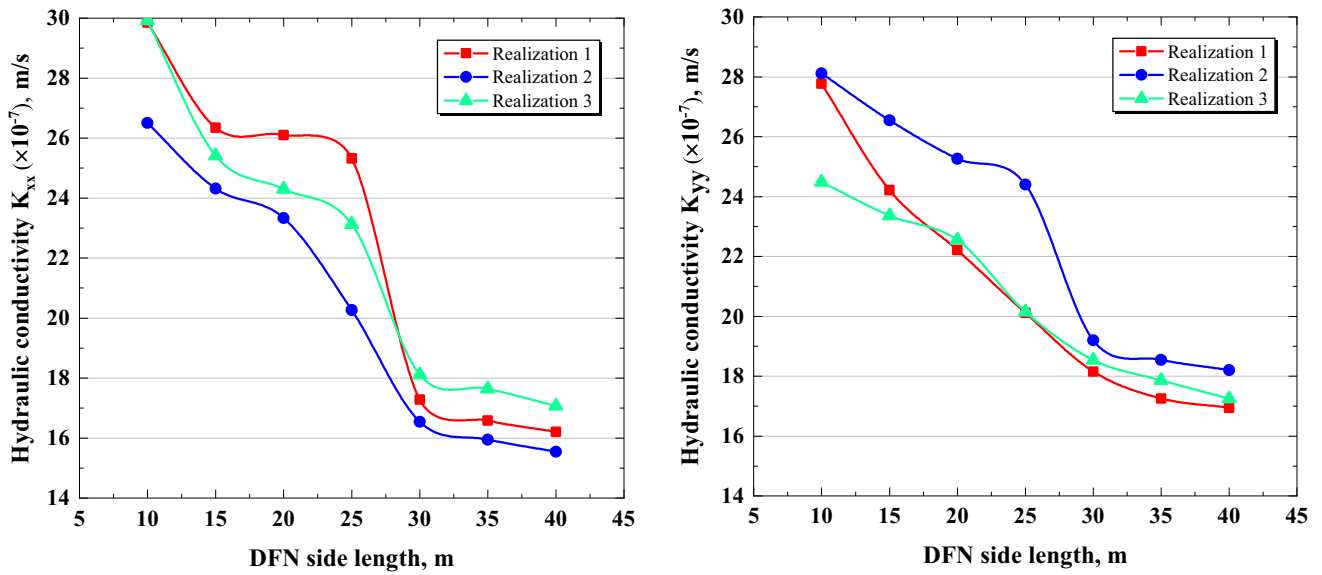


Fig. 12 Hydraulic conductivity (K_{xx} and K_{yy}) with F.D = 1.2

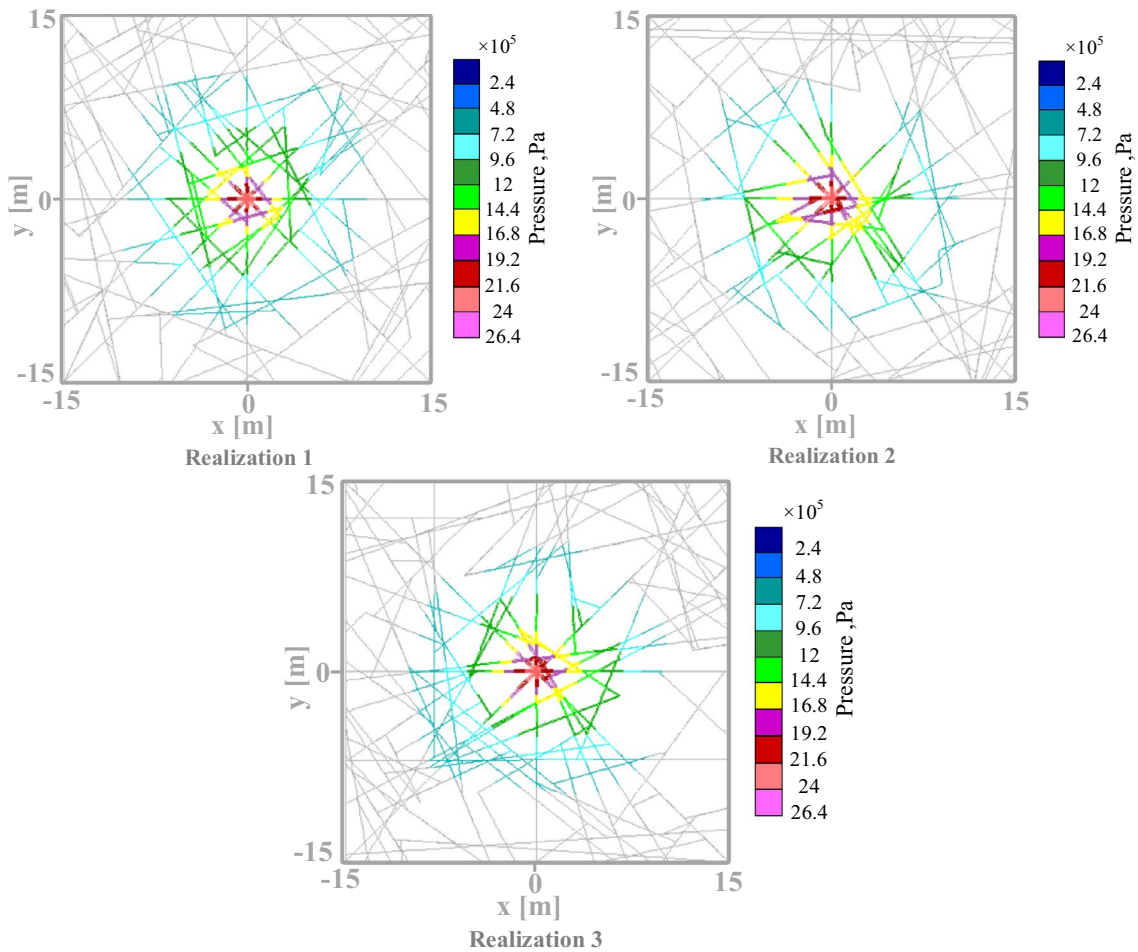


Fig. 13 Propagation pattern in fracture networks with F.D=0.4

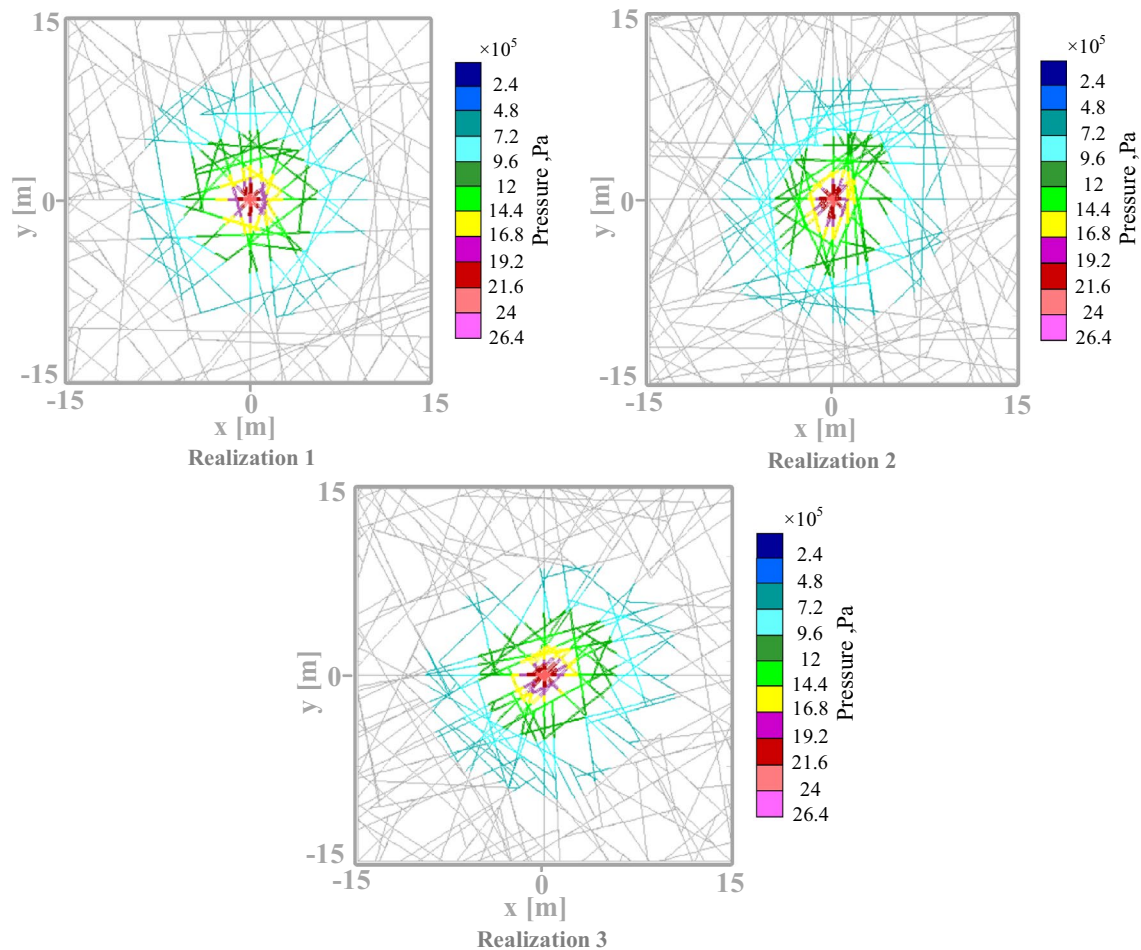


Fig. 14 Propagation pattern in fracture networks with F.D=0.8

($\approx 1.5 D_{\text{tunnel}}$). Because the distance of the injected grout pressure from the tunnel wall does not cause damage to the segments installed in the tunnel wall. When there is not much water leakage, and the depth of the injection hole is 4 m, the entire length of the hole can be injected at once by installing a packer in the hole. However, when there is a lot of water leakage, and 7 m holes are drilled for injection, the length of the hole is divided into two sections of 3 m and 4 m. The first 3 m of the hole, which is close to the surface, will be injected with low pressure and the last 4 m of the hole with higher pressure.

The injection pressure has been calculated using different equations, ranging from 1.2 to 7 bar, based on the length of injection boreholes for sealing injection in zone HG11 of the KWCT (see Table 3). As shown in this table, the maximum injection pressure is obtained based on European criteria. For injection boreholes with a depth of 7 m, the average injection pressure of about 4 bar has been considered for use in numerical and analytical solutions. Additionally, the water pressure should be considered 20 bar in zone HG11 of the northern lot of the tunnel. Therefore, the

injection pressure should be greater than the water pressure ($P_g > 20$ bar). For this purpose, 24 bar (4 + 20 bar) has been applied to overcome hydrostatic pressure in numerical and analytical solutions.

Results of DFN-DEM Numerical Analysis

Generation of DFN Realizations Using the Stochastic Approach

To reduce the random effect, discrete element method (DEM) softwares including 3DEC version 5.0 and UDEC version 6.0 were used to stochastically generate various DFN realizations. In this study, the location and orientation of fractures were determined using the uniform and fisher distribution functions [30]. The largest and smallest fracture lengths and length distribution exponent (α) were used based on the power-law distribution to be 100 m, 1 m, and 3, respectively. A total of nine different fracture network realizations were generated using three fracture densities

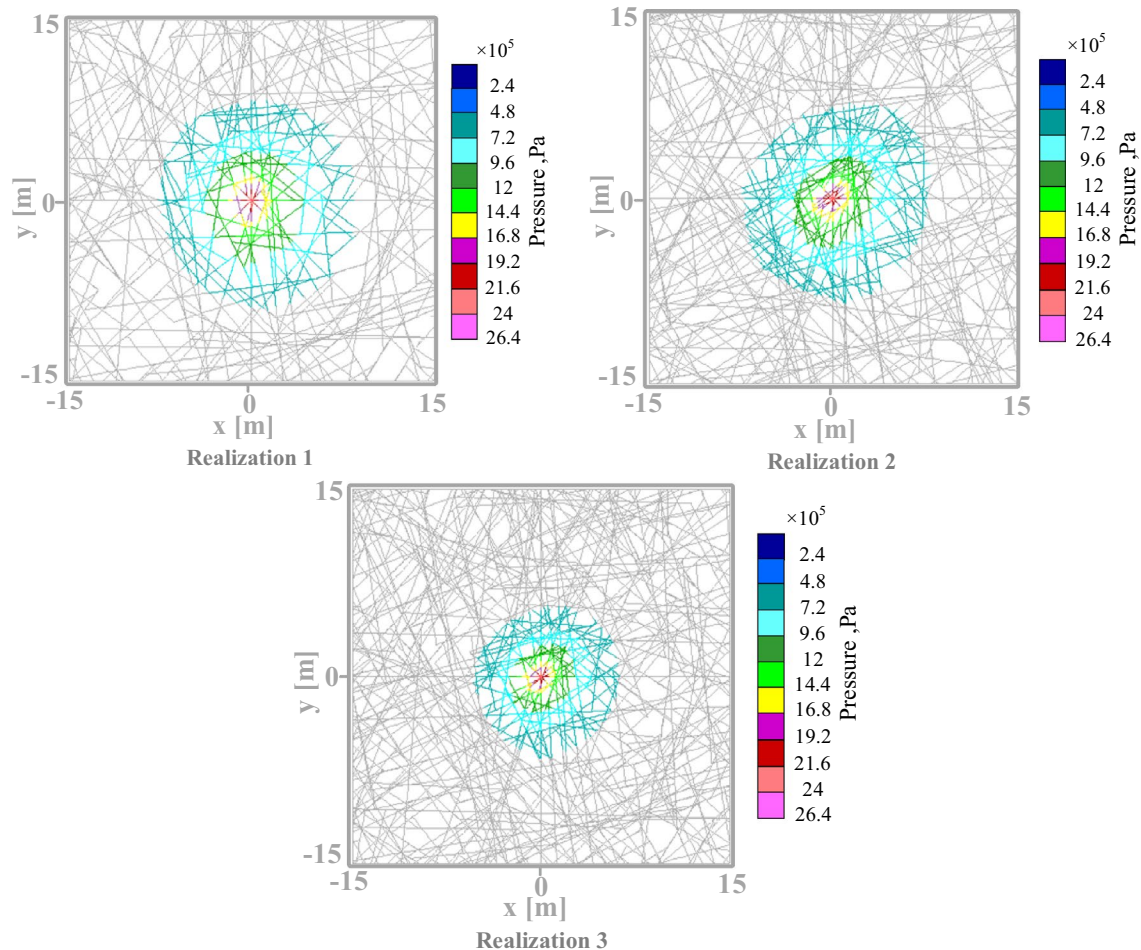


Fig. 15 Propagation pattern in fracture networks with F.D=1.2

of 0.4 m^{-2} , 0.8 m^{-2} , and 1.2 m^{-2} . The basic properties of fractures of zone HG11 in the KWCT are shown in Table 4. The different realizations of the fracture networks randomly generated at different densities are shown in Fig. 8.

In addition to the random effect, the uncertainty associated with the boundary effect of the fracture network must also be reduced. For this purpose, to evaluate the equivalent hydraulic behaviors, the effect of model size on the equivalent permeability of fracture networks should be estimated based on the concept of Representative Elementary Volume (REV). The hydraulic REV for fractured rocks defines the minimum volume of a sampling domain beyond which the permeability of the sampling domain remains largely constant [17]. Hence, when the sizes of DFN models are higher

than their REVs, the equivalent properties will become scale-independent.

Using 50 m as the block side length, Fig. 9 shows the generated DFNs extracted from the 3D model in 3DEC and transformed into the 2D model in UDEC. In 3DEC software, the joints can be cut and extracted in the desired direction by considering the dip and direction of the cutting plane. In this study, all joint cutting planes have been extracted in the Dip = 90° and Dip Direction = 0° .

Calculation of the Hydraulic Conductivity and REV Size in the 2D Cut Plane

Many studies have shown that the permeability of the jointed rock mass is completely dependent on the REV size of the

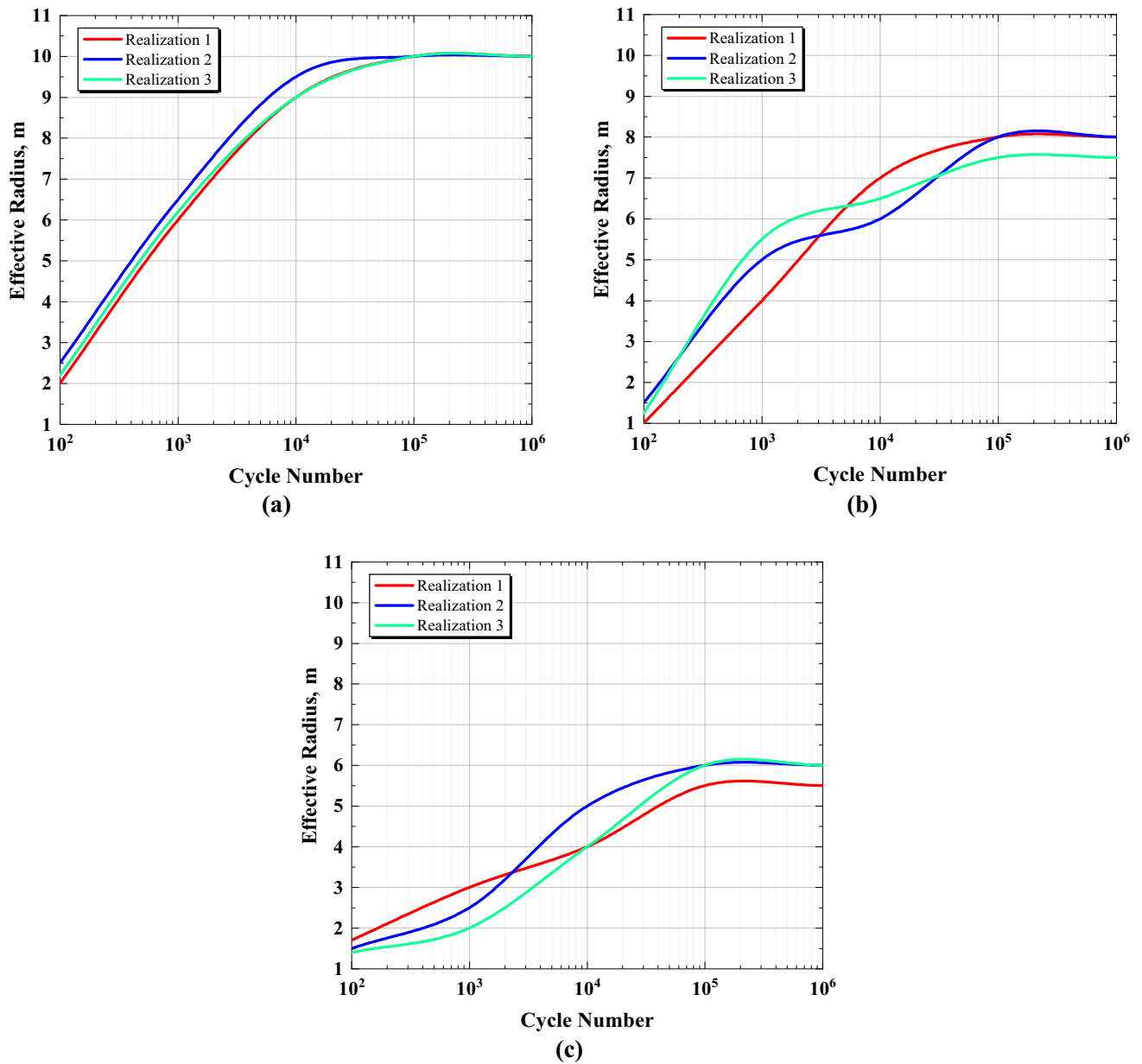
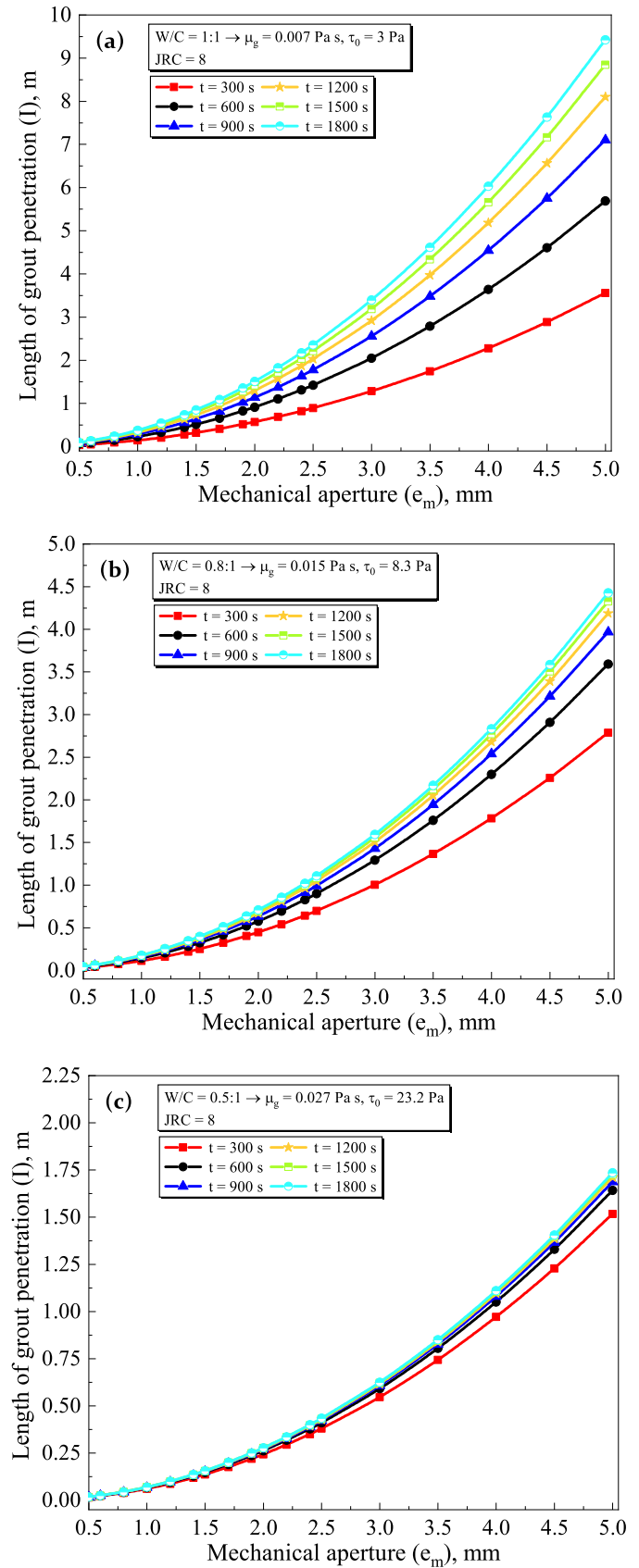


Fig. 16 The effective radius of grout in different realizations of fracture networks with **a** F.D=0.4 **b** F.D=0.8, **c** F.D=1.2

fracture network [19, 30, 31]. So, determining the REV size is the first step in the hydraulic analyses of the rock mass. In other words, it is necessary to determine the optimal size of the blocks to determine the hydraulic properties of the rock mass using DFN analysis. This work is done using the generation of different realizations.

After generating suitable models using the DFN-DEM approach and applying hydraulic boundary conditions, the hydraulic conductivity of the rock mass is calculated according to Darcy’s law. Blocks of different dimensions were examined to eliminate the scale effect on the values of hydraulic properties. For 2D models, the dimensions of the

Fig. 17 Variation of grout penetration length with respect to the aperture, viscosity, yield value, and injection time; $\Delta P = 4 \times 10^5$ Pa, JRC = 8



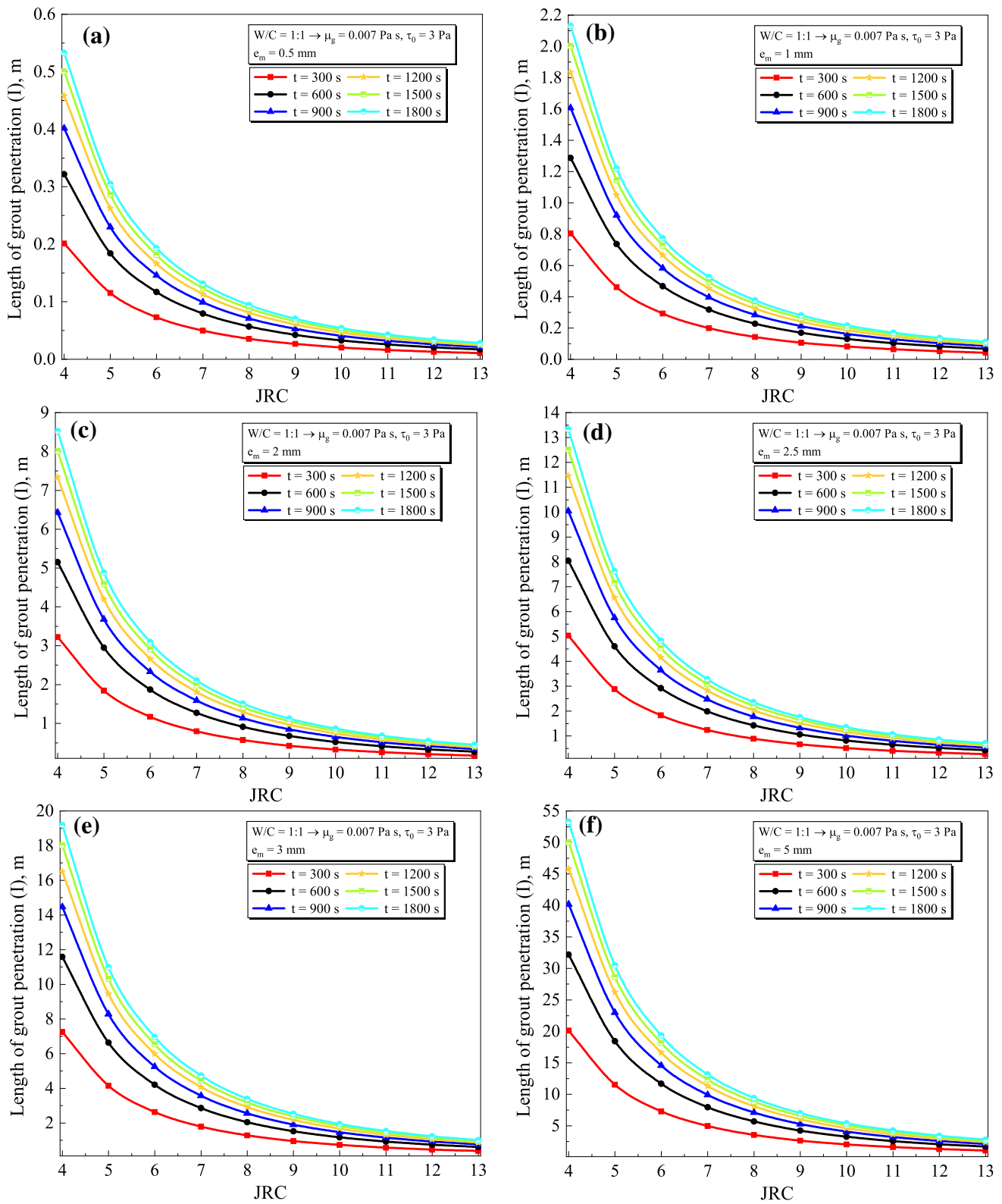


Fig. 18 Variation of grout penetration length with respect to the JRC, aperture, and injection time; $\Delta P = 4 \times 10^5 \text{ Pa}, \mu_g = 0.007 \text{ Pa s}, \tau_0 = 3 \text{ Pa}$

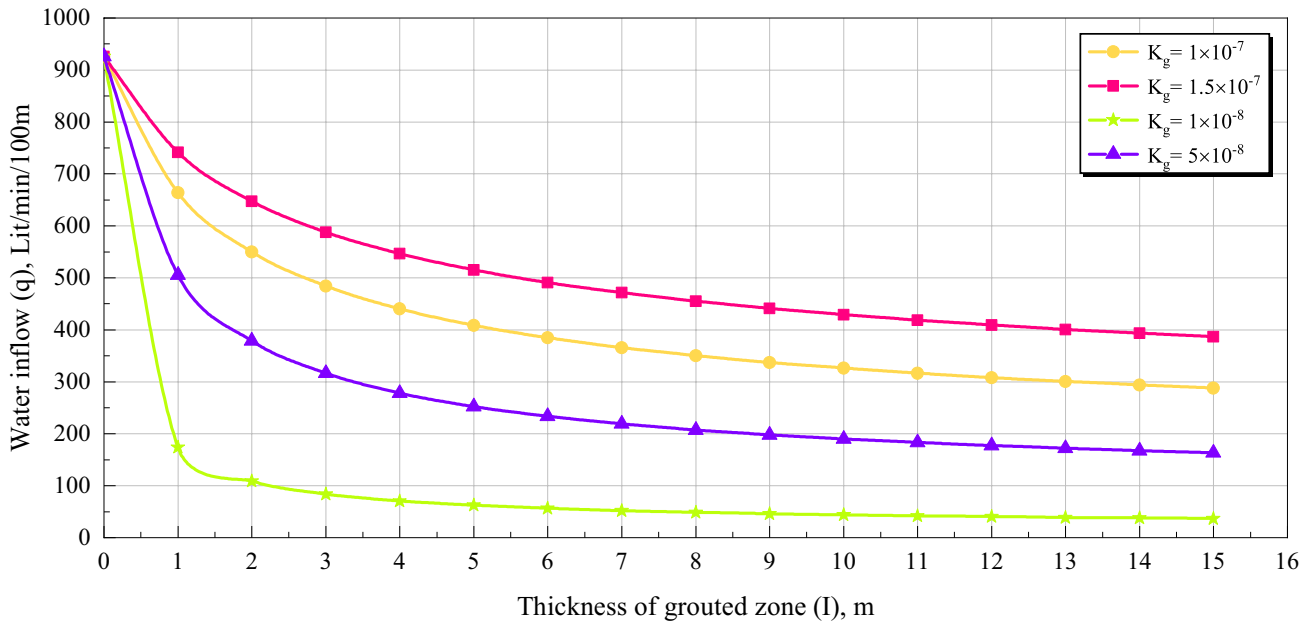


Fig. 19 Water inflow to the grouted KWCT as a function of the conductivity and the thickness of the grouted zone ($H=200$ m, $R_l = 2.33$ m, $\xi=3$, and initial conductivity = 1×10^{-6} m/s)

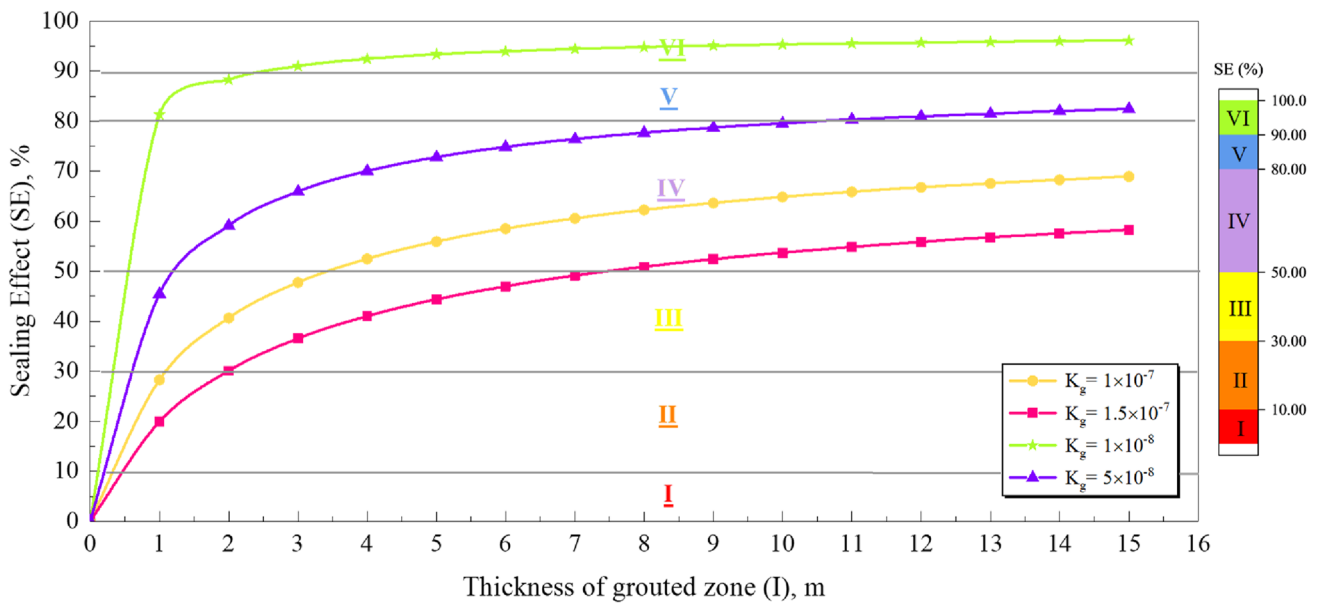


Fig. 20 Calculated sealing effect for grouted KWCT project ($H=200$ m, $R_l = 2.33$ m, $\xi=3$, initial conductivity = 1×10^{-6} m/s, and allowable inflow = 120 Lit/min/100 m)

blocks with side lengths of 10, 15, 20, 25, 30, 35, and 40 m were extracted from the blocks of 50 m.

Figures 10, 11, 12 show the results of calculated values of permeability elements K_{xx} and K_{yy} from the nine random realizations with different fracture densities at different model sizes. The calculated permeability components

become smaller as the model size increases, and the permeability values maintain constant ranges after a specific size. As can be seen, after 30 m, the permeability values in both the x and y directions begin to approach each other, and the values of K_{xx} and K_{yy} take a constant trend. Hence, this size can be approximated as the REV size for future

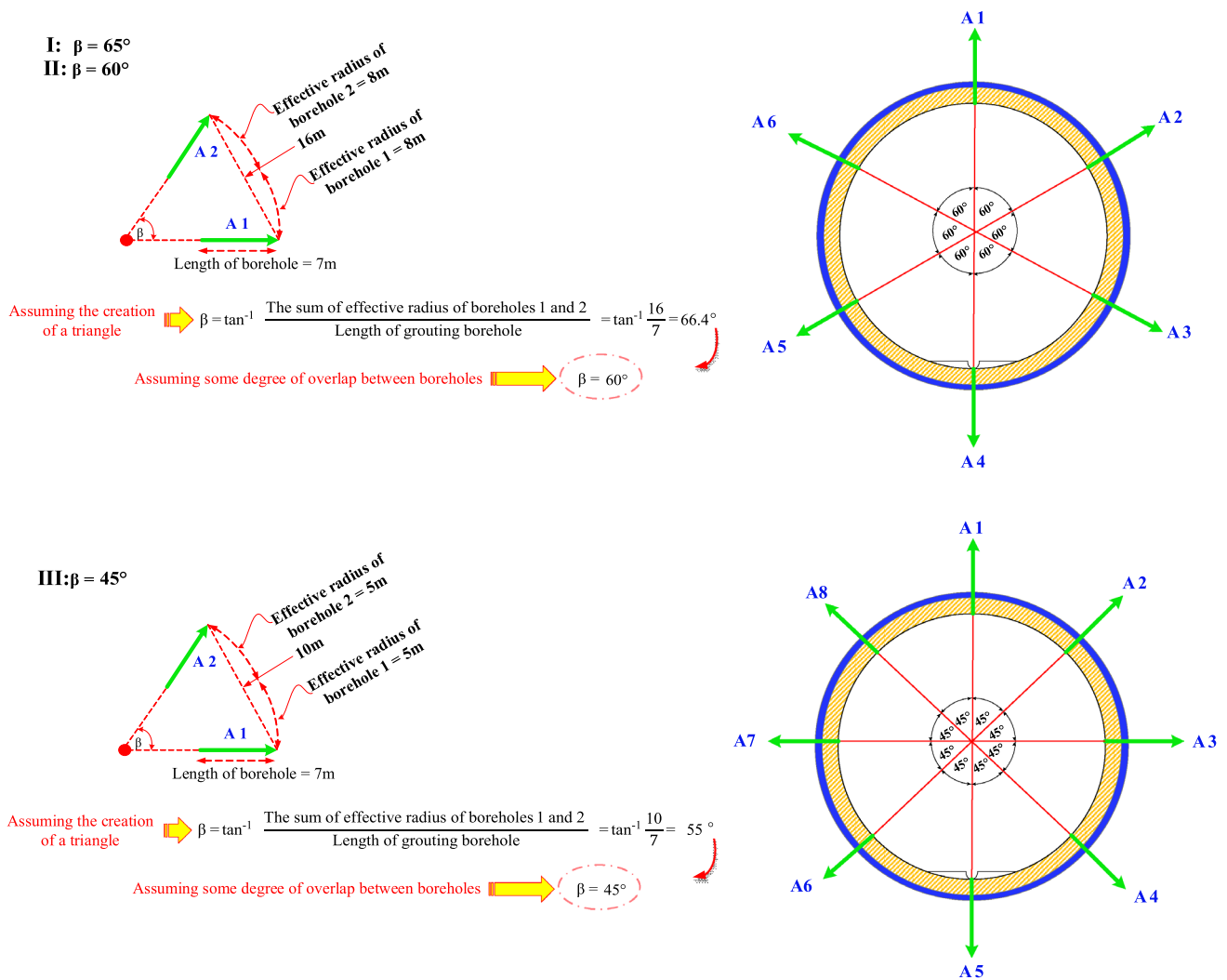


Fig. 21 Determination of the angle between adjacent injection holes on a concrete segment

analysis, including the effective radius of the grout and the suitable pattern of the injection boreholes in zone HG11 of the KWCT project.

Grout Propagation and Determination of the Effective Radius

In this section, the results obtained from the numerical simulation of the grouting process of zone HG11 are presented. The required parameters of the injection process must be determined before modeling the cement propagation and calculating its effective radius in the jointed rock mass. The most important parameters for estimating the effective radius in numerical modeling are determining the grouting pressure and selecting the cement grout mix design.

The purpose of these simulations is to obtain the injected grout's propagation so that the two adjacent injection boreholes overlap each other to achieve sealing. For this purpose, the grout injection process was simulated in nine separate fracture networks with different fracture densities (F.D) in $30 \times 30 \text{ m}^2$ dimensions, with an injection borehole in the center of the models with a diameter of 56 mm and 24 bar injection pressure.

As shown in Figs. 13, 14, 15, the grout propagation in the rock mass decreases as the fracture density of the fracture networks increases. In other words, the grout effective radius decreases as the number of fractures increases. It should be noted that in numerical simulations, the effective radius increases with the increasing number of numerical cycles until the effective radius number of the cycles curve is fixed. As shown in Fig. 16, the maximum effective

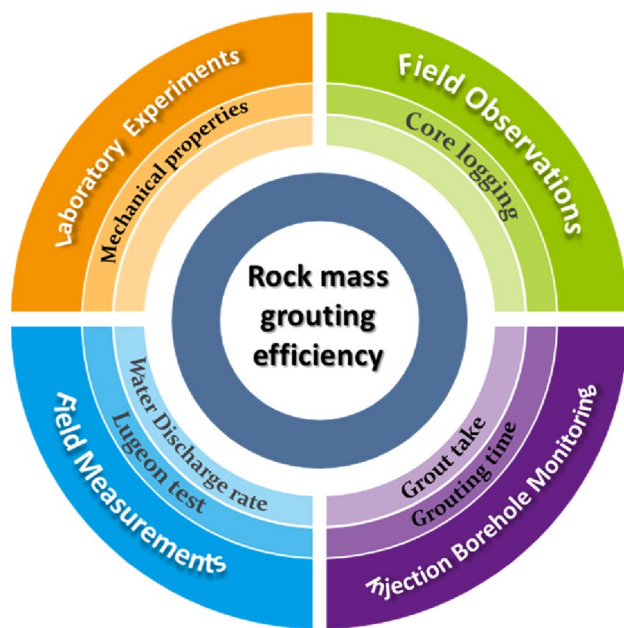


Fig. 22 Some methods of evaluating the efficiency of rock mass grouting in the tunnel

radius values of the grout in fracture networks with fracture densities of 0.4, 0.8, and 1.2, are about 10 m, 8 m, and 5 m, respectively. However, with increasing fracture density, the grout penetration area becomes more symmetrical. Therefore, with the symmetry of the grout penetration area, it can be said that the grout injection operation is more suitable in terms of performance. Furthermore, the amount of grout pressure applied in the holes decreases radially around the injection holes in their center.

Determination of Length of Grout Penetration by Analytical Solutions

In addition to the DFN-DEM approach, the analytical solution of Gustafson and Stille [24] was used to further investigate the grout penetration length [Eqs. (9)–(13)]. The majority of the joints in the HG11 zone of KWCT were in the 1–5 mm range, and analyses were done on these apertures (joints are in the open and moderately wide classes based on ISRM standard [32]). Also, three types of grouts with different W/C ratios (or different viscosities and yield values) were used in the analyses. Grouts with W/C ratios of 0.5:1, 0.8:1, and 1:1 have viscosities of 0.027, 0.015, and 0.007 Pa s, respectively. Figure 17(a–c) shows how progressively the grout penetration length can be nonlinearly varied along with the mechanical aperture. Figure 17(c) also shows that using grouts with a lower W/C ratio (higher viscosity)

reduces the length of grout penetration in joints. On the other hand, the use of grouts with a higher water-to-cement ratio also reduces the yield shear strength of the grout (τ_0). As a result, grouts with a W/C ratio of 1:1 can be used to begin the injection operations and increase the grout penetration length. Furthermore, it is clear that the grout penetration length is higher in joints with larger apertures. The penetration length in the joints can also be increased by increasing the injection time.

The roughness and aperture of a rock joint are the most important factors governing fluid flow through the joint [10]. Roughness is an important factor in both mechanical and hydraulic behavior [33]. For this purpose, in this study, changes in grout penetration length were investigated in six constant apertures of 0.5, 1, 2, 2.5, 3, and 5 mm at different injection times and JRC values of the KWCT zone HG11, which ranges from 4 to 13. As can be seen in Fig. 18(a)–(f), the grout penetration length decreases with increasing JRC and is approximately constant after JRC = 8. In other words, these figures show that after JRC = 8, the grout penetration length decreases with a smaller slope. Therefore, it can be concluded that in KWCT zones where JRC values are less than 8, the injection time can be increased to increase the grout penetration length.

After determining the grout penetration length using numerical and analytical solutions, the sealing effect can be evaluated based on different grout penetration lengths. This was accomplished using Eqs. (6)–(8). Figure 19 shows the predicted amount of water inflow into the tunnel at various hydraulic conductivity values and different thicknesses of the grouted zone. As shown in this figure, creating a grouted zone with a thickness of 3 m will have a significant effect on reducing the water inflow into the KWCT. When the grouted zone is increased to about 6 m thick, the amount of water inflow into the tunnel is reduced. But injecting more than about 6 m will not lead to a significant reduction in water inflow into the tunnel and will increase the cost of injection operations. On the other hand, the quality of the injection operations can be improved by carefully executing the injection process and selecting grout with the ability to penetrate properly into the smallest joints. It may be necessary to use more expensive finely ground cement like UFC (ultra-fine) or MFC (micro-fine) in these cases [34]. In other words, hydraulic conductivities of around 10^{-8} m/s can be achieved using very fine cement. It should be noted that the allowable discharge rate in the KWCT project is 120 Lit/min/100 m. As a result, very fine cement must be used to achieve the permissible discharge rate in KWCT as shown in Fig. 19. In this case, by injecting a grout with a thickness of 5 m into

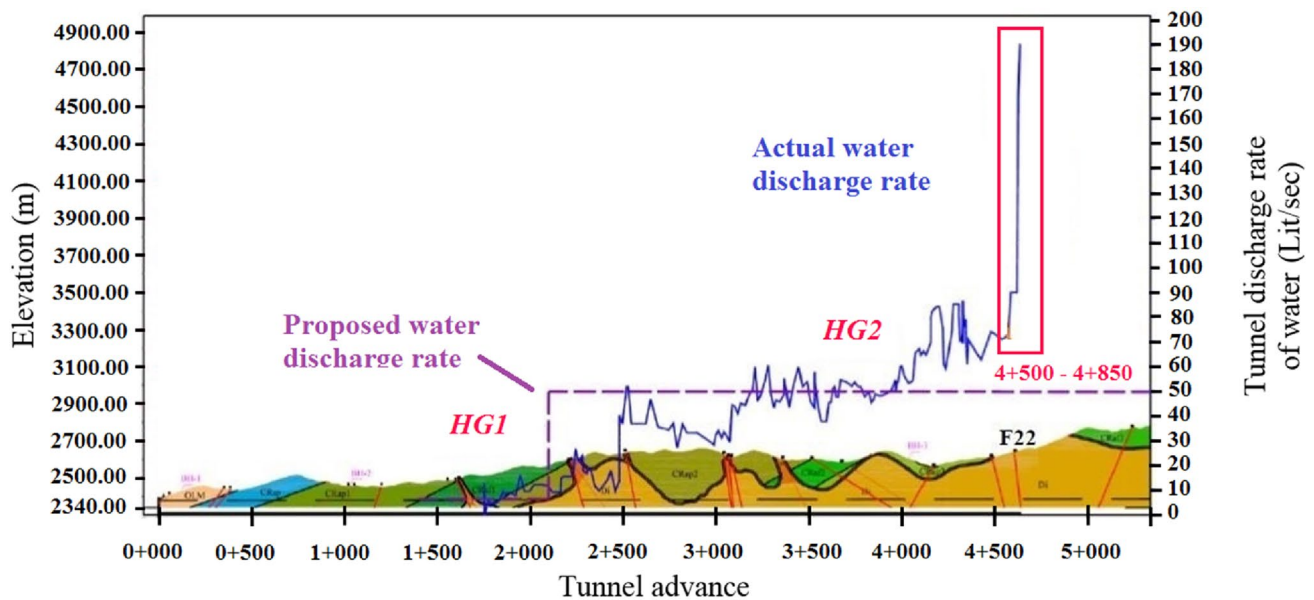


Fig. 23 Actual values of water inflow into the tunnel in the southern portal and water inrush into the tunnel

the tunnel, the discharge rate into the tunnel is reduced to less than 60 Lit/min/100 m.

Figure 20 shows the sealing effect (SE) for different grouted zone thicknesses. As shown in this figure, the sealing effect values increase with the increasing thickness of the grouted zone and are nearly constant from one thickness onward. Furthermore, the sealing effect is exceeding 90% from a grouted zone thickness of approximately 5 m onwards in order to obtain hydraulic conductivity of roughly 10^{-8} m/s. In this case, it can be said that the injection operation was of high quality. However, as demonstrated in Fig. 20, achieving a larger sealing effect at a hydraulic conductivity of 10^{-7} m/s is difficult.

Determination of the Suitable Injection Arrangement

The angle between two adjacent injection boreholes can be calculated after determining the grout's effective radius in fracture networks with various densities. Injection boreholes should be located on a segmental ring of the KWCT based on the grout's effective radius. By considering the average effective radius of 8 m and 5 m for two adjacent injection holes, the angles of the first series injection boreholes can be determined (see Fig. 21). As a result of the calculations in Fig. 21(I) and (II), the drilling angles of holes in rock

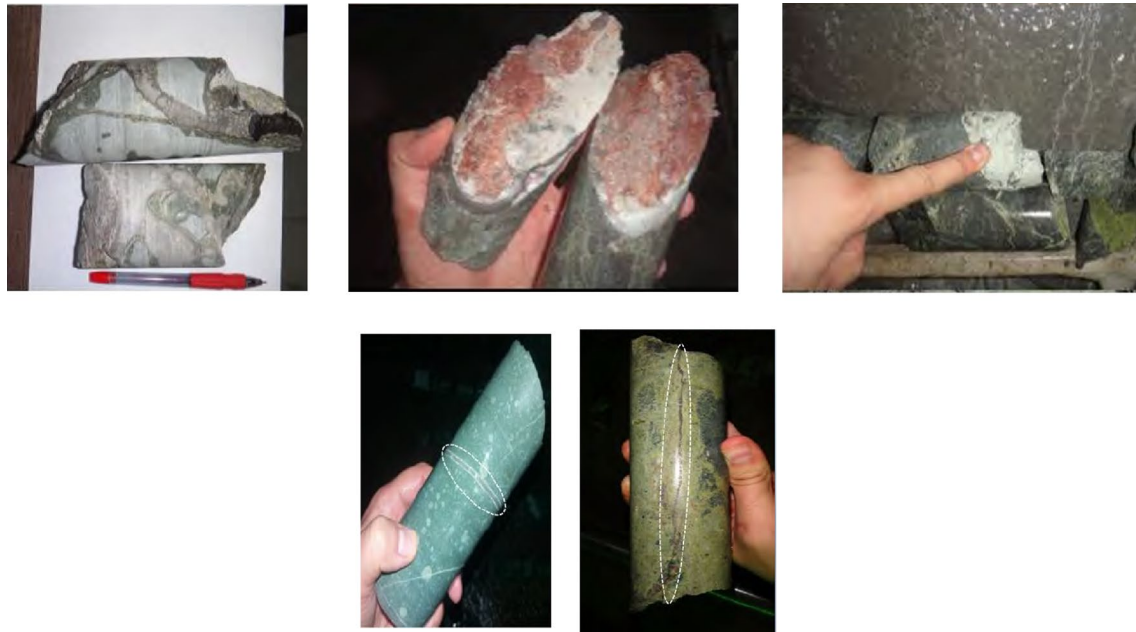


Fig. 24 Monitoring of the core samples from injected boreholes

masses with fracture densities of 0.4 and 0.8 are approximately 70.71° and 66.4° , respectively. However, due to some overlaps in the design of the injection borehole arrangement, it is suggested that the injection holes be angled at 60° . The injection boreholes on a ring of the concrete segment were also placed according to the obtained optimal angle, as shown in Fig. 21. As can be seen in this figure, in rock masses with fracture densities of 0.4 and 0.8, six injection boreholes with angles of 60° relative to each other are located on a segmental ring with a width of 1.3 m. Furthermore, the arrangement of the boreholes can be used according to Fig. 21(III) in zones of the tunnel route where water inflow into the tunnel is high or there is a fault. The injection boreholes will overlap well with these arrangements, creating a zone in the tunnel environment and, as a result, reducing water inflow from the springs surrounding the tunnel.

In general, grouting mainly serves to improve the watertightness, strength, and stability of the surrounding ground [35]. To achieve the above goals, there are several methods for evaluating the performance of the grout injection process. These techniques can be divided into four categories (see Fig. 22). The first method involves evaluating the mechanical properties of rock samples before and after injection operations using control or check holes. For example, P-wave velocity and strength can be measured and justified before and after injection operations. The second method involves measuring the water discharge rate and Lugeon values before and after the injection operation. The injection process can also be evaluated on-site by evaluating the filling of cement grout in the joints and cracks of core

samples. Finally, the injection operation can be controlled based on the amount of cement grout consumed and the injection time.

After designing the arrangement of injection holes in the zones with high water inflow, in order to investigate the proposed arrangement efficiency, the injection operations were studied in one of the sections of the southern lot of the tunnel that had a fault. During the excavation of TBM in the southern lot (4 + 570 to 4 + 721 km) and the collision with fault F22, the springs in the area were affected and the volume of water inflow into the tunnel increased significantly. As shown in Fig. 23, Fault F22 in zone HG2 has significantly increased water inflow into the tunnel. Therefore, the injection was performed to reduce the water inflow into the tunnel. According to the proposed arrangement, the injection operation was performed in the studied section. Figure 24 shows some rock core samples before and after grouting. After the grouting, some boreholes were selected to evaluate the grouting efficiency and to check the filling condition of the solidified grout in the cracks of the rock mass. According to pressure filtration theory [36], grouting can be divided into two stages, filling and saturation. During the filling stage, the slurry enters and fills large parts of the cracks. During the subsequent saturation stage, excess water in the slurry is injected into the smaller cracks or pores under the saturation pressure [37]. The bottom parts of Fig. 24 show that the solidified grout penetrates the cracks in the rock mass. During the grouting diffusion process, the grouting pressure replaces the initial gap width of the crack as the main control factor affecting the grout diffusion radius

[37]. Therefore, after the injection, the grout inside the joints strengthened the rock mass, indicating that the injection was successful.

Conclusions

In the current paper, numerical modeling of the appropriate arrangement of injection boreholes in the HG11 zone rock mass of the Kerman water conveyance tunnel (KWCT) project was performed using the DFN-DEM and analytical approaches. The grout's effective radius of a studied zone in the northern part of the tunnel was obtained after creating discrete fracture networks (DFNs) with different fracture densities, which were also calculated with analytical solutions. Based on the obtained results, modeling of grout injection operations was performed in several stages, and finally, a suitable grouting pattern was designed. Based on the findings, the following conclusions are made:

- The results showed that as the block dimensions increased, the rate of hydraulic conductivity changes tended to stabilize at a constant level in blocks with dimensions of $30 \times 30 \text{ m}^2$. This dimension is considered as a representative elementary volume (REV) for future analyses, such as determining the grout's effective radius and the suitable arrangement of injection boreholes.
- The maximum effective radius of the grout in fracture networks with fracture densities of 0.4, 0.8, and 1.2 was found to be 10, 8, and 5 m, respectively. By considering the effective radius of 10 m and 8 m for two adjacent injection boreholes, the angles between the two injection boreholes are about 60° .
- The angle between the two injection boreholes is calculated to be about 45° in zones of the tunnel route where water inflow into the tunnel is high, there is a fault, and fracture density is also high.
- In addition to numerical modeling, two analytical models were used to determine the grout penetration length and sealing effect (SE). Based on the results of analytical models, it was found that the optimal grout penetration length is about 5 m, with a sealing effect of more than 90% in this case.
- Furthermore, the results of in situ injection operations of the southern lot of the tunnel, which was exposed to water inrush from the fault, were analyzed. After the grouting, some boreholes were selected to evaluate the grouting efficiency and to check the filling condition of the solidified grout in the cracks of the rock mass. The observations indicate that the proposed arrangements are highly efficient.

Finally, the approaches and the techniques presented in this study will assist other similar projects in better planning for sealing problems and designs.

Data Availability All data generated and analyzed during this study are included in this article.

Declarations

Conflict of Interest The authors declare that they have no known competing financial interests or personal relationships that could have appeared to influence the work reported in this paper.

References

1. Mao D, Lu M, Zhao Z, Ng M (2016) Effects of water related factors on pre-grouting in hard rock tunnelling. *Procedia Eng* 165:300–307. <https://doi.org/10.1016/j.proeng.2016.11.704>
2. Kim H-M, Lee J-W, Yazdani M et al (2018) Coupled viscous fluid flow and joint deformation analysis for grout injection in a rock joint. *Rock Mech Rock Eng* 51:627–638. <https://doi.org/10.1007/s00603-017-1339-3>
3. Stille H (2015) *Rock grouting: theories and applications*. BeFo-Rock Engineering Research Foundation, Stockholm
4. Ma H, Yin L, Gong Q, Wang J (2015) TBM tunneling in mixed-face ground: problems and solutions. *Int J Min Sci Technol* 25:641–647. <https://doi.org/10.1016/j.ijmst.2015.05.019>
5. Tóth Á, Gong Q, Zhao J (2013) Case studies of TBM tunneling performance in rock–soil interface mixed ground. *Tunn Undergr Sp Technol* 38:140–150. <https://doi.org/10.1016/j.tust.2013.06.001>
6. Zhao J, Gong QM, Eisensten Z (2007) Tunnelling through a frequently changing and mixed ground: a case history in Singapore. *Tunn Undergr Sp Technol* 22:388–400. <https://doi.org/10.1016/j.tust.2006.10.002>
7. Kobayashi S, Stille H (2007) Design for rock grouting based on analysis of grout penetration. Verification using Äspö HRL data and parameter analysis. Swedish Nuclear Fuel and Waste Management Co
8. Ghafar AN, Montesidis A, Draganovic A, Larsson S (2016) An experimental approach to the development of dynamic pressure to improve grout spread. *Rock Mech Rock Eng* 49:3709–3721. <https://doi.org/10.1007/s00603-016-1020-2>
9. Butrón C, Gustafson G, Fransson Å, Funehag J (2010) Drip sealing of tunnels in hard rock: a new concept for the design and evaluation of permeation grouting. *Tunn Undergr Sp Technol* 25:114–121. <https://doi.org/10.1016/j.tust.2009.09.008>
10. Saeidi O, Stille H, Torabi SR (2013) Numerical and analytical analyses of the effects of different joint and grout properties on the rock mass groutability. *Tunn Undergr Sp Technol* 38:11–25. <https://doi.org/10.1016/j.tust.2013.05.005>
11. Mortazavi A, Maadikhah A (2016) An investigation of the effects of important grouting and rock parameters on the grouting process. *Geomech Geoeng* 11:219–235. <https://doi.org/10.1080/17486025.2016.1145255>
12. Mohajerani S, Baghbanan A, Wang G, Forouhandeh SF (2017) An efficient algorithm for simulating grout propagation in 2D discrete fracture networks. *Int J Rock Mech Min Sci* 98:67–77. <https://doi.org/10.1016/j.ijrmms.2017.07.015>
13. Zou L, Håkansson U, Cvetkovic V (2019) Cement grout propagation in two-dimensional fracture networks: impact of structure and

- hydraulic variability. *Int J Rock Mech Min Sci* 115:1–10. <https://doi.org/10.1016/j.ijrmms.2019.01.004>
14. Gustafson G, Claesson J, Fransson Å (2013) Steering parameters for rock grouting. *J Appl Math* 2013:1–9. <https://doi.org/10.1155/2013/269594>
 15. Zou L, Håkansson U, Cvetkovic V (2018) Two-phase cement grout propagation in homogeneous water-saturated rock fractures. *Int J Rock Mech Min Sci* 106:243–249. <https://doi.org/10.1016/j.ijrmms.2018.04.017>
 16. Janson T, Stille H, Hakansson U (1994) Grouting of jointed rock—a case study, Department of Soil and Rock Mechanics, Royal Institute of Technology. Stockholm, Sweden
 17. Khani A, Baghbanan A, Hashemolhosseini H (2013) Numerical investigation of the effect of fracture intensity on deformability and REV of fractured rock masses. *Int J Rock Mech Min Sci*. <https://doi.org/10.1016/j.ijrmms.2013.08.006>
 18. Lei Q, Latham J-P, Tsang C-F (2017) The use of discrete fracture networks for modelling coupled geomechanical and hydrological behaviour of fractured rocks. *Comput Geotech* 85:151–176. <https://doi.org/10.1016/j.compgeo.2016.12.024>
 19. Karbalaee MA, Katibeh H (2009) Cement grouting in Rocks. Tarava, Ahvaz (**In Persian**)
 20. Zhang X, Sanderson DJ, Harkness RM, Last NC (1996) Evaluation of the 2-D permeability tensor for fractured rock masses. *Int J Rock Mech Min Sci Geomech Abstr* 33:17–37. [https://doi.org/10.1016/0148-9062\(95\)00042-9](https://doi.org/10.1016/0148-9062(95)00042-9)
 21. Wilkinson WL (1960) Non-Newtonian fluids: fluid mechanics, mixing and heat transfer. Pergamon Press, London
 22. Dalmalm T (2004) Choice of grouting method for jointed hard rock based on sealing time predictions. Doctoral dissertation, Department of Civil and Architectural Engineering, Royal Institute of Technology
 23. Eriksson M, Stille H (2005) Cementinjektering i hart berg (In Swedish). SveBeFo Report K22, Swedish Rock Engineering Research, Stockholm
 24. Gustafson G, Stille H (2005) Stop criteria for cement grouting. *Felsbau* 23:62–68
 25. Gholizadeh H, Peely AB, Karney BW, Malekpour A (2020) Assessment of groundwater ingress to a partially pressurized water-conveyance tunnel using a conduit-flow process model: a case study in Iran. *Hydrogeol J* 28:2573–2585. <https://doi.org/10.1007/s10040-020-02213-y>
 26. Barton N, Bandis S, Bakhtar K (1985) Strength, deformation and conductivity coupling of rock joints. *Int J Rock Mech Min Sci Geomech Abstr* 22:121–140. [https://doi.org/10.1016/0148-9062\(85\)93227-9](https://doi.org/10.1016/0148-9062(85)93227-9)
 27. Olsson R, Barton N (2001) An improved model for hydromechanical coupling during shearing of rock joints. *Int J rock Mech Min Sci* 38:317–329. [https://doi.org/10.1016/S1365-1609\(00\)00079-4](https://doi.org/10.1016/S1365-1609(00)00079-4)
 28. Rosquoët F, Alexis A, Khelidj A, Phelipot A (2003) Experimental study of cement grout: rheological behavior and sedimentation. *Cem Concr Res* 33:713–722. [https://doi.org/10.1016/S0008-8846\(02\)01036-0](https://doi.org/10.1016/S0008-8846(02)01036-0)
 29. El Tani M (2012) Grouting rock fractures with cement grout. *Rock Mech rock Eng* 45:547–561. <https://doi.org/10.1007/s00603-012-0235-0>
 30. Min K-B, Jing L, Stephansson O (2004) Determining the equivalent permeability tensor for fractured rock masses using a stochastic REV approach: method and application to the field data from Sellafeld, UK. *Hydrogeol J* 12:497–510. <https://doi.org/10.1007/s10040-004-0331-7>
 31. Baghbanan A, Jing L (2007) Hydraulic properties of fractured rock masses with correlated fracture length and aperture. *Int J Rock Mech Min Sci* 44:704–719. <https://doi.org/10.1016/j.ijrmms.2006.11.001>
 32. ISRM (1978) suggested methods for the quantitative description of discontinuities in rock masses. *Int J Rock Mech Min Sci Geomech Abstr* 15:319–368. [https://doi.org/10.1016/0148-9062\(78\)91472-9](https://doi.org/10.1016/0148-9062(78)91472-9)
 33. Bandis SC, Lumsden AC, Barton NR (1983) Fundamentals of rock joint deformation. *Int J Rock Mech Min Sci Geomech Abstr* 20:249–268. [https://doi.org/10.1016/0148-9062\(83\)90595-8](https://doi.org/10.1016/0148-9062(83)90595-8)
 34. Barton N, Quadros E (2019) Understanding the need for pre-injection permeability measurements: what is the connection? *J Rock Mech Geotech Eng* 11:576–597. <https://doi.org/10.1016/j.jrmge.2018.12.008>
 35. Zhang D, Fang Q, Lou H (2014) Grouting techniques for the unfavorable geological conditions of Xiang'an subsea tunnel in China. *J Rock Mech Geotech Eng* 6:438–446. <https://doi.org/10.1016/j.jrmge.2014.07.005>
 36. Attneave F, Arnoult MD (1956) The quantitative study of shape and pattern perception. *Psychol Bull* 53:452. <https://doi.org/10.1037/h0044049>
 37. Dou J, Zhang G, Zhou M et al (2020) Curtain grouting experiment in a dam foundation: case study with the main focus on the Lugeon and grout take tests. *Bull Eng Geol Environ* 79:4527–4547. <https://doi.org/10.1007/s10064-020-01865-0>

Publisher's Note Springer Nature remains neutral with regard to jurisdictional claims in published maps and institutional affiliations.

Springer Nature or its licensor (e.g. a society or other partner) holds exclusive rights to this article under a publishing agreement with the author(s) or other rightsholder(s); author self-archiving of the accepted manuscript version of this article is solely governed by the terms of such publishing agreement and applicable law.